European Journal of Medicinal Chemistry 267 (2024) 116167

Contents lists available at ScienceDirect

European Journal of Medicinal Chemistry

journal homepage: www.elsevier.com/locate/ejmech

Research paper

Design, synthesis, and biological characterization of proteolysis targeting chimera (PROTACs) for the ataxia telangiectasia and RAD3-related (ATR) kinase

Abdallah M. Alfayomy [a,b,1], Ramy Ashry [c,d,1], Anita G. Kansy [c], Anne-Christin Sarnow [a], Frank Erdmann [a], Matthias Schmidt [a], Oliver H. Krämer [c,2,**], Wolfgang Sippl [a,2,*]

[a] Department of Medicinal Chemistry, Institute of Pharmacy, Martin-Luther-University of Halle-Wittenberg, 06120, Halle (Saale), Germany
[b] Department of Pharmaceutical Chemistry, Faculty of Pharmacy, Al-Azhar University, Assiut, 71524, Egypt
[c] Department of Toxicology, University Medical Center, Johannes Gutenberg-University Mainz, 55131, Mainz, Germany
[d] Department of Oral Pathology, Faculty of Dentistry, Mansoura University, Mansoura, 35516, Egypt

ARTICLE INFO

Handling editor: Z Liu

Keywords:
Ataxia telangiectasia and RAD3-Related (ATR) kinase
Proteolysis targeting chimera (PROTAC)
Protein degradation
Synthesis
MIA PaCa-2

ABSTRACT

The Ataxia telangiectasia and RAD3-related (ATR) kinase is a key regulator of DNA replication stress responses and DNA-damage checkpoints. Several potent and selective ATR inhibitors are reported and four of them are currently in clinical trials in combination with radio- or chemotherapy. Based on the idea of degrading target proteins rather than inhibiting them, we designed, synthesized and biologically characterized a library of ATR-targeted proteolysis targeting chimera (PROTACs). Among the synthesized compounds, the lenalidomide-based PROTAC **42i** was the most promising. In pancreatic and cervix cancer cells cancer cells, it reduced ATR to 40 % of the levels in untreated cells. **42i** selectively degraded ATR through the proteasome, dependent on the E3 ubiquitin ligase component cereblon, and without affecting the associated kinases ATM and DNA-PKcs. **42i** may be a promising candidate for further optimization and biological characterization in various cancer cells.

1. Introduction

Chemotherapeutics induce DNA replication stress and DNA damage. If such lesions are not repaired, they cause cell death. Exogenously induced and endogenous DNA replication problems and DNA lesions activate checkpoint kinases, which slow down the cell cycle and initiate DNA repair [1–3]. The checkpoint kinases ataxia telangiectasia-mutated (ATM) and checkpoint kinase-2 (CHK2) are mainly activated in cells with double-strand DNA breaks. DNA replication stress, due to slow or blocked DNA replication forks and single-strand DNA breaks, activates Ataxia telangiectasia and RAD3-related (ATR) and checkpoint kinase-1 (CHK1). DNA-dependent protein kinase catalytic subunit (DNA-PKcs) is, like ATM and ATR, an apical checkpoint kinase immediately sensing DNA stress [2,3].

The coordination of cellular responses to DNA replication stress and endangered DNA integrity by checkpoint kinase has propelled an intense search for pharmacological inhibitors of such enzymes [4,5]. In particular, ATR kinase has attracted interest, as cancer cells are heavily rely on ATR to cope with the increased amount of replication stress, and also mutations in ATR are less common [3,6,7]. A first potent and selective inhibitor for ATR, **I** (VE-821), was reported by Vertex Pharmaceuticals [8]. The inhibitor is highly selective for ATR compared to its homologous kinases ATM and DNA-PKcs. Preclinical studies have shown that **I** (VE-821) is able to sensitize multiple tumor cell lines to various treatments, including cisplatin, ionizing radiation, gemcitabine, topoisomerase I poisons, etoposide, and oxaliplatin [9–11]. Although it was effective at inhibiting ATR, it lacked pharmacokinetic properties needed to advance into clinical trials [8,12]. Several optimizations have been made on this scaffold to increase the potency and cellular activity against ATR and to improve its physicochemical properties. For instance, the isosteric replacement of the amide with a 1,3,4-oxadiazole (**IIa**) or isoxazole moiety (**IIb**) increased the cellular activity against ATR

* Correspondence to.
** Correspondence to.
E-mail addresses: okraemer@uni-mainz.de (O.H. Krämer), wolfgang.sippl@pharmazie.uni-halle.de (W. Sippl).
[1] equal first author contribution.
[2] contributed equally

https://doi.org/10.1016/j.ejmech.2024.116167
Received 9 November 2023; Received in revised form 12 January 2024; Accepted 21 January 2024
Available online 29 January 2024

[12]. Further modifications led to the discovery of another candidate **III (**VX-970, also known as VE-822**)** with improved potency, selectivity, and water solubility, which is currently in phase II clinical trials [12–14] (Fig. 1).

Proteolysis targeting chimeras (PROTACs) have emerged as a highly promising new strategy for the development of future drugs [15–17]. These heterobifunctional molecules consist of a ligand which binds to the target protein of interest, a ligand binding to an E3 ubiquitin ligase (such as cereblon, CRBN, or von Hippel–Lindau tumor suppressor, VHL), and a linker connecting both ligands. PROTACs initiate the degradation of their targets by inducing the formation of a ternary complex with an E3 ligase. This directs the ubiquitination machinery close to the protein. The polyubiquitinated protein is consequently recognized and degraded by the 26S proteasome. Studies have shown several advantages of PROTACs over the corresponding small molecule inhibitors, including increased potency, rapid and sustained depletion of the targeted proteins, and enhanced selectivity in cells [18,19]. Eighteen protein degraders are currently in phase I to III clinical trials for the treatment of tumor patients [20,21]. So far, targeted protein degraders (TPDs) have not been reported for the checkpoint kinases ATR, ATM, DNA-PKcs, CHK1, and CHK2. Such compounds would represent an innovative pharmacology to dissect and therapeutically assess the catalytic and non-catalytic functions of these key molecular regulators [22]. Herein, we report the chemical synthesis and biological characterization of the first-in-class degraders for ATR kinase through the application of the PROTAC concept.

2. Results and discussion

2.1. Docking study

We started the design of ATR PROTACs based upon the ATR inhibitors **I,** its analog **IIa,** and **III.** The interaction between the inhibitors and ATR kinase was analyzed by docking study. Some ATR inhibitors have been cocrystallized with a rationally designed PI3K-alpha mutant that mimics ATR (PDB ID 5UL1) [23]. In addition, a cryo-EM structure has been reported for the apo-form of the human ATR/ATRIP complex (PDB-ID: 5YZ0) [24]. We used this structure to generate a 3D model of the inhibitor-bound form of human ATR/ATRIP which was then compared with the PI3K-alpha mutant that mimics ATR. The ATP-binding site of both proteins shows 61.3 % sequence similarity and 43.5 % identity. Only few residues that interact with the inhibitors are different in both structures, e.g. Thr856 that makes a hydrogen bond with the sulfone moity in the PI3K-alpha mutant is changed to Gly2385 in the ATR/ATRIP model structure. Further differences are reported in Table S1 in the Supplement.

In the PI3K-alpha mutant crystal structure **I** occupies the ATP binding site and forms two hydrogen bonds between the 2-aminopyrazine moiety and the hinge region while the alkyl sulfone group protrudes into the solvent-exposed region of the protein. Docking of **I**, **IIa**, **III** (VE-822) as well the sulfonamide analog **13g** to the PI3K-alpha mutant crystal structure as well as to the generated ATR/ATRIP model gave a similar orientation of the 2-aminopyrazine and sulfone groups (Figs. 2 and 3). Based on the structural information the sulfone group is proposed as feasible tethering site for connecting a linker group. The published in vitro data of inhibitor **IIa** and **IIb** [12] showed the same inhibitory activity with an IC_{50} of approximately 1 nM. The cellular activity of **IIa** was about three times stronger compared to **IIb**. Therefore, in the current work, we used the 1,3,4-oxadizaole scaffold of **IIa** in addition to scaffold **I** and introduced the alkylamine group reported for inhibitor **III** into both scaffolds. Additionally, different E3 ligase ligands such as several cereblon ligands (thalidomide, lenalidomide, and other glutarimides) and VHL-ligand were considered for the PROTAC development using different alkyl and PEG linkers with variant linker lengths (Fig. 4).

2.2. Chemistry

The designed PROTACs were prepared via a convergent synthesis, including condensation between linker-connected ATR inhibitors (**12a-e** and **13a-f)** and different E3 ligase ligands (**20a-c, 25, 31, 35** and **41**), as outlined in Schemes 1-5. The synthetic routes for the linker-connected ATR inhibitors were illustrated in Scheme 1. Firstly, the 4-bromobenzene sulfonyl chloride **2** reacted with different alkyl and PEG linkers **1a-f** and with methyl amine **1g** to form the corresponding 4-bromobenzene sulfonamide derivatives **3a-g**. Secondly, 4-bromobenzene sulfonamides with alkyl linkers **3a-d** were converted to the corresponding boronates **4a-d** through the Miyaura borylation reaction by cross-coupling with bis(pinacolato)diboron [25]. Concurrently, ester hydrolysis of methyl 3-amino-6-bromopyrazine-2-carboxylate **8** with lithium hydroxide gives the corresponding acid **9** [8]. Then, the carboxylic acid group of the produced pyrazine carboxylic acid **9** either reacted with different benzohydrazides in the presence of triphenylphosphine and carbon tetrabromide to afford the 2-phenyl-1,3,4-oxadiazole derivative **10a, b** or was coupled with aniline through a HATU-mediated coupling reaction to form the corresponding carboxamide derivative **11a** [12,26]. The benzohydrazide derivative **7,** which was required for the synthesis of the oxadiazole derivative **10b,** was synthesized starting from the corresponding substituted methyl benzoate **5** by N-methylation with methyl iodide in the presence of sodium hydride, followed by reaction with hydrazine hydrate in methanol, affording the corresponding benzohydrazide derivative **7**. Furthermore, the pyrazine carboxamide **11a** was converted to the corresponding pinacol boronic ester **11b** through the Miyaura borylation reaction, followed by coupling with the intermediate **3g** using the Suzuki cross-coupling reaction to get the modified ATR inhibitor **13g** [25,27]. Finally, cross-coupling of bromoaryl intermediates **3e, 3f, 10a, b** and **11a** with the appropriate pinacolate boronic ester derivatives **4a-d** and **11b** using the Suzuki cross-coupling reaction followed by ester hydrolysis either by trifluoracetic acid for *t*-butyl ester or lithium hydroxide for methyl ester afforded the linker-connected ATR inhibitors **12a-e** and **13a-f**.

On the other hand, several cereblon (CRBN) warheads were prepared based on the structures of the reported cereblon ligands lenalidomide, thalidomide, and other glutarimides. The lenalidomide-based ligands were prepared as described in Scheme 2. First, a radical brominating reaction occurred between methyl 3-bromo-2-methyl benzoate **14** and NBS in the presence of benzoyl peroxide to give the corresponding 2-bromomethyl derivative **15,** which was further reacted with 3-aminopiperidine-2,6-dione **16** in the presence of triethylamine to yield the lenalidomide derivative **17a** [28,29]. Then, the latter was methylated with methyl iodide using potassium carbonate as a base to give the corresponding *N*-methylated analog **17b** (which will be used for the

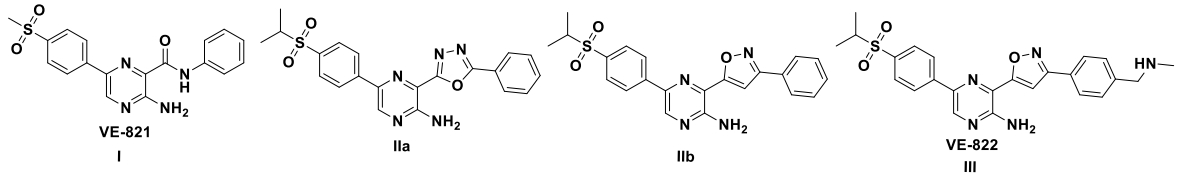

Fig. 1. Examples of reported ATR inhibitors that were used in this work for the development of PROTACs.

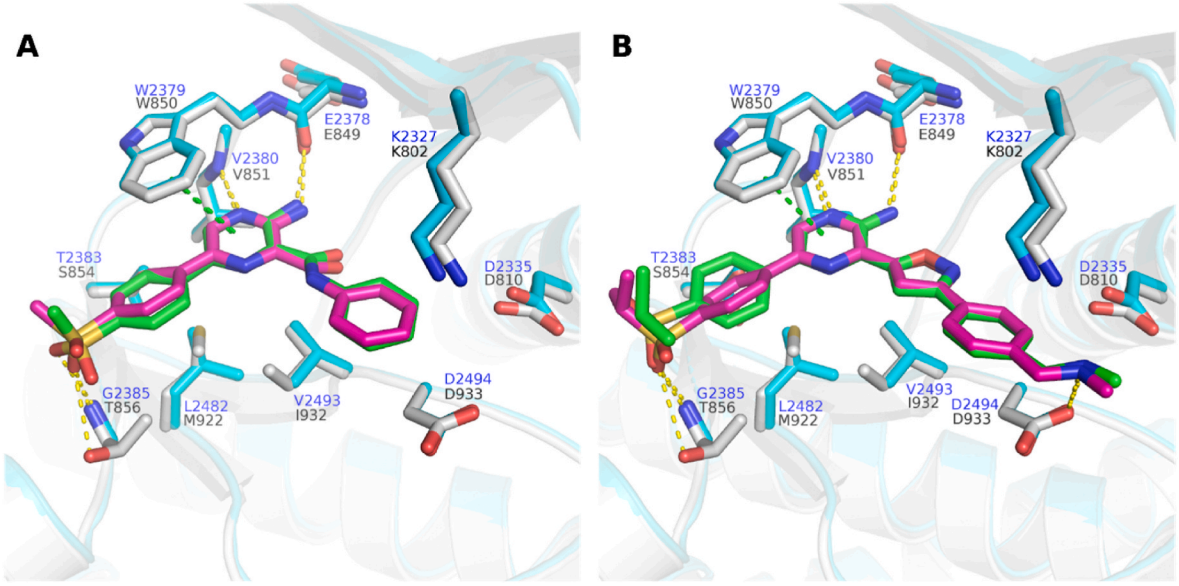

Fig. 2. Obtained docking poses of **I** (VE821) (**A**) and **III** (VE822) (**B**) in PDB 5UL1 and the ATR homology model. The protein backbone is represented as white cartoon (PDB 5UL1) or cyan cartoon (ATR model). Important binding site residues are shown as white sticks (PDB 5UL1) or cyan sticks (ATR model). ATR inhibitors are represented in stick representation and their carbon atoms are colored pink (docking pose in PDB 5UL1) or green (docking pose in the ATR homology model). Hydrogen bonds are shown as yellow dashed lines and π−π interactions in green dashed lines.

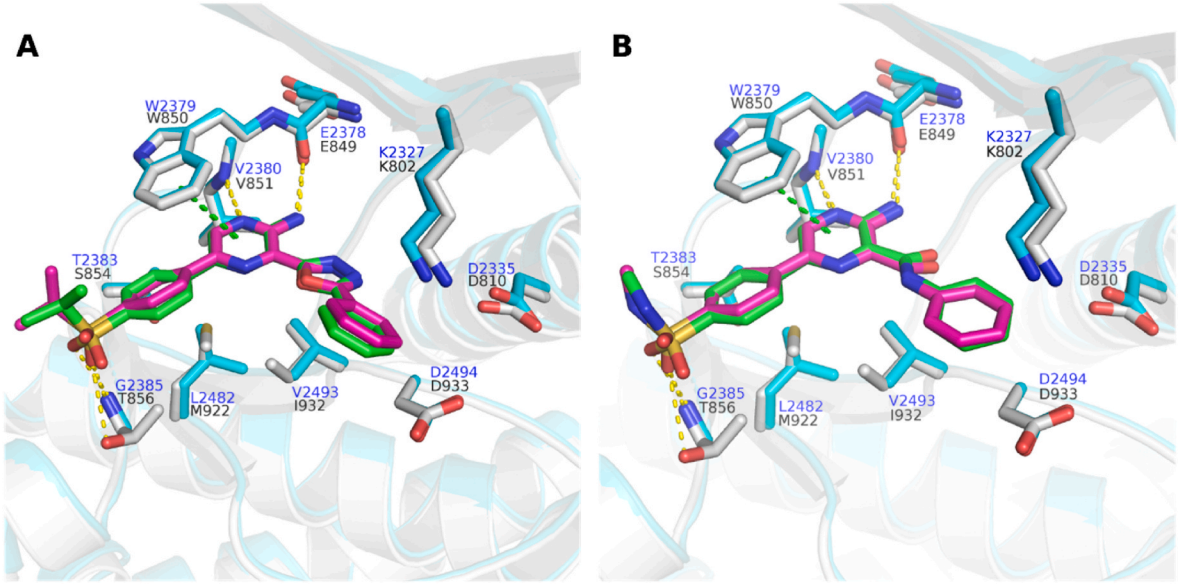

Fig. 3. Obtained docking poses of **IIa** (**A**) and **13g** (**B**) in PDB 5UL1 or the ATR homology model. The protein backbone is represented as white cartoon (PDB 5UL1) or cyan cartoon (ATR model). Important binding site residues are shown as white sticks (PDB 5UL1) or cyan sticks (ATR model). ATR inhibitors are represented in stick representation and their carbon atoms are colored pink (docking pose in PDB 5UL1) or green (docking pose in the ATR homology model). Hydrogen bonds are shown as yellow dashed lines and π−π interactions in green dashed lines.

negative control synthesis) [29]. Finally, intermediates **20a-c** were synthesized by Sonogashira coupling reactions between the compounds **17a, b** and terminal alkyne linkers **18a, b** followed by Boc-deprotection under acidic conditions [30].

Also, the thalidomide-based cereblon ligand **25** was synthesized as shown in Scheme 3. The 4-fluorophthalic anhydride **21** was reacted with 3-aminopiperidine-2,6-dione **16** to afford the 5-flurothalidomide **22,** which was then converted to its piperazine analog **24** through its reaction with 1-Boc-piperazine **23,** followed by Boc-deprotection to afford the thalidomide analog **25** [29,31]. In addition, the synthetic pathway for the phenyl-glutarimide derivative **28** was illustrated in Scheme 4. The 3-bromopyridine derivative **26** was coupled with 4-hydroxyphenyl boronic acid **27** using the Suzuki cross-coupling condition to afford the corresponding 3-phenylpyridine derivative **28** [32]. Then, the hydroxyl group of intermediate **28** was alkylated with *N*-Boc-2-bromoethylamine to produce the corresponding alkylated derivative **29**. Finally, a palladium-catalyzed hydrogenation reaction is used to remove the two benzyl groups and saturate the pyridine ring, followed by Boc-de protection under acidic condition, affording the phenyl-glutarimide derivative **31** [32]. Furthermore, the picolinamide glutarimide derivative **35** was synthesized according to Scheme 4. The 6-fluoropicolinic acid **32** was coupled with 3-aminopiperidine-2,6-dione **16** to afford the 6- fluoropicolinamide derivative **33,** which was then converted to its piperazine analog **34** through its reaction with 1-Boc-piperazine **23,**

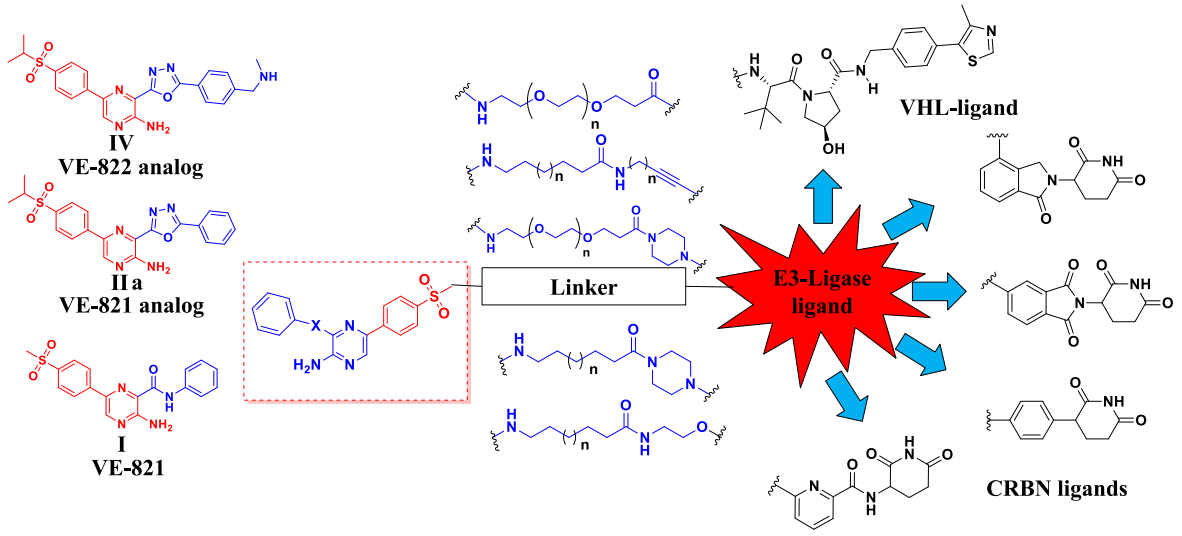

Fig. 4. Strategy for design of ATR PROTACs.

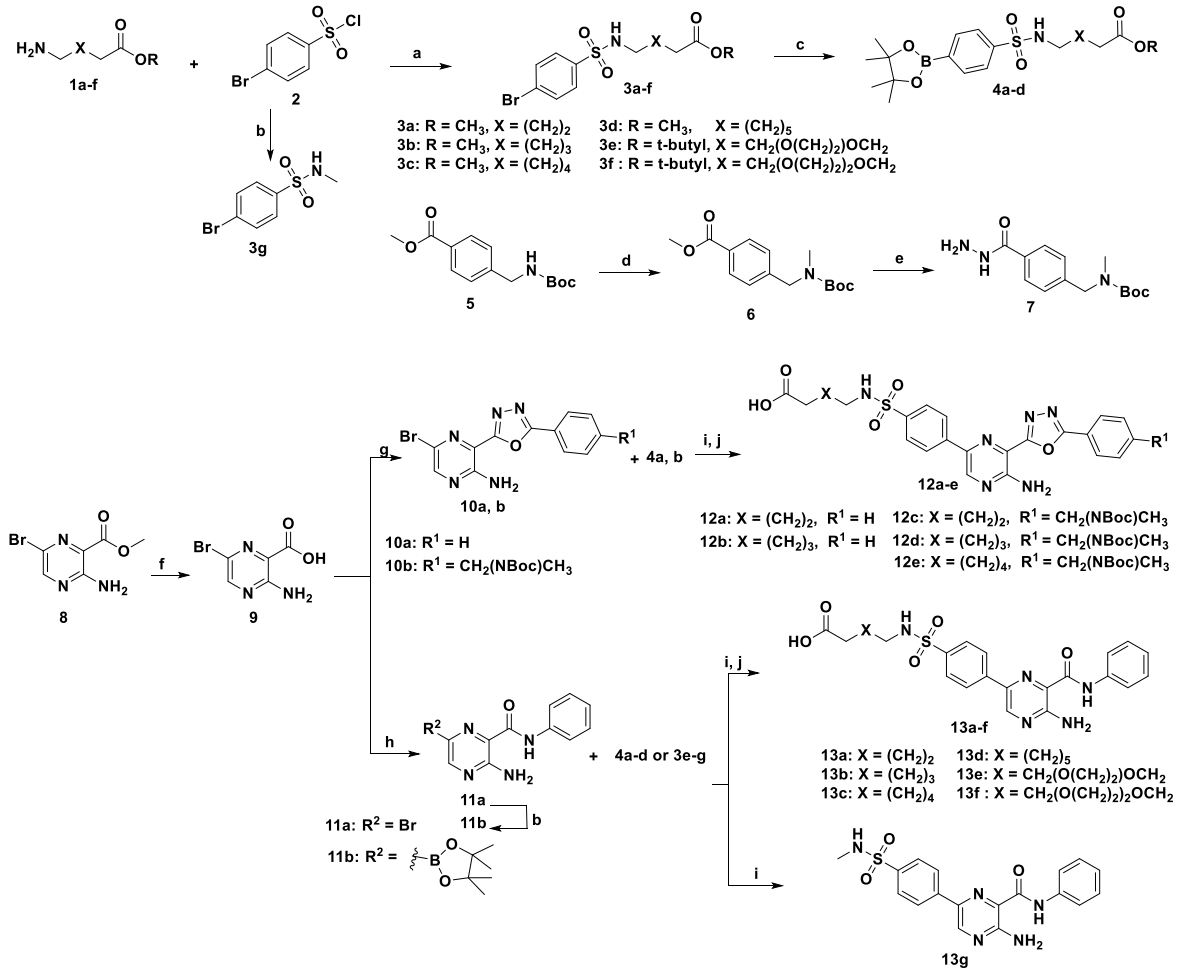

Scheme 1. Reagents and conditions: (a) TEA, Acetonitrile (b) Methyl amine **1g**, $NaHCO_3$ EtOAc, H_2O (c) B_2pin_2, $Pd(dppf)Cl_2$ KOAc, Dioxan (d) CH_3I, NaH, DMF (e) $NH_2NH_2.H_2O$, CH_3OH (f) LiOH, H_2O, CH_3OH (g) Benzohydrazides, PPh_3, CBr_4, TEA (h) Aniline, HATU, DIPEA, DMF (i) $Pd(dppf)Cl_2$ Na_2CO_3, Dioxan, H_2O (j) For methyl esters: LiOH, H_2O, THF. For *t*-butyl esters: DCM, TFA.

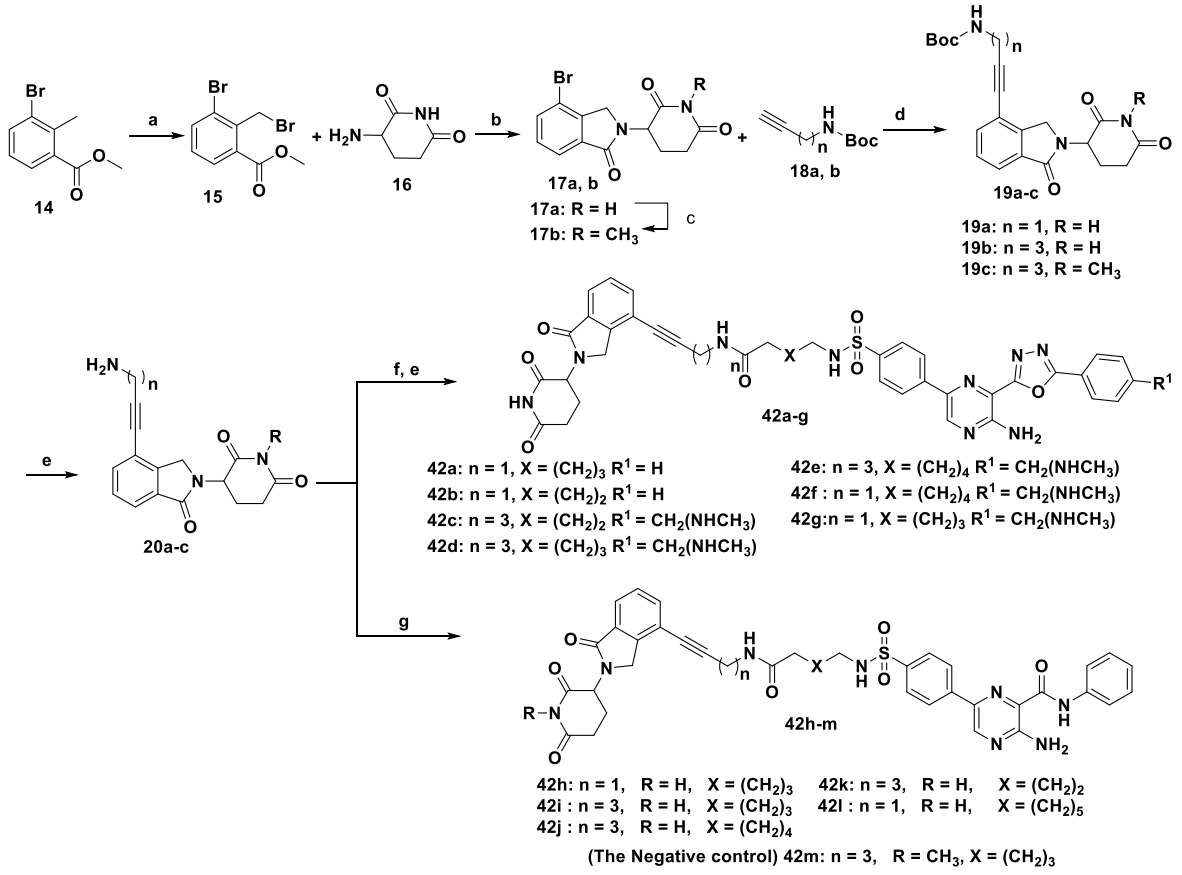

Scheme 2. Reagents and conditions: (a) NBS, BPO, CCl_4 (b) TEA, Acetonitrile (c) CH_3I, K_2CO_3, DMF (d) $Pd(dpp)_2Cl_2$ TEA, DMF (e) DCM, TFA (f) **12a-e**, HATU, DIPEA, DMF (g) **13a-f**, HATU, DIPEA, DMF.

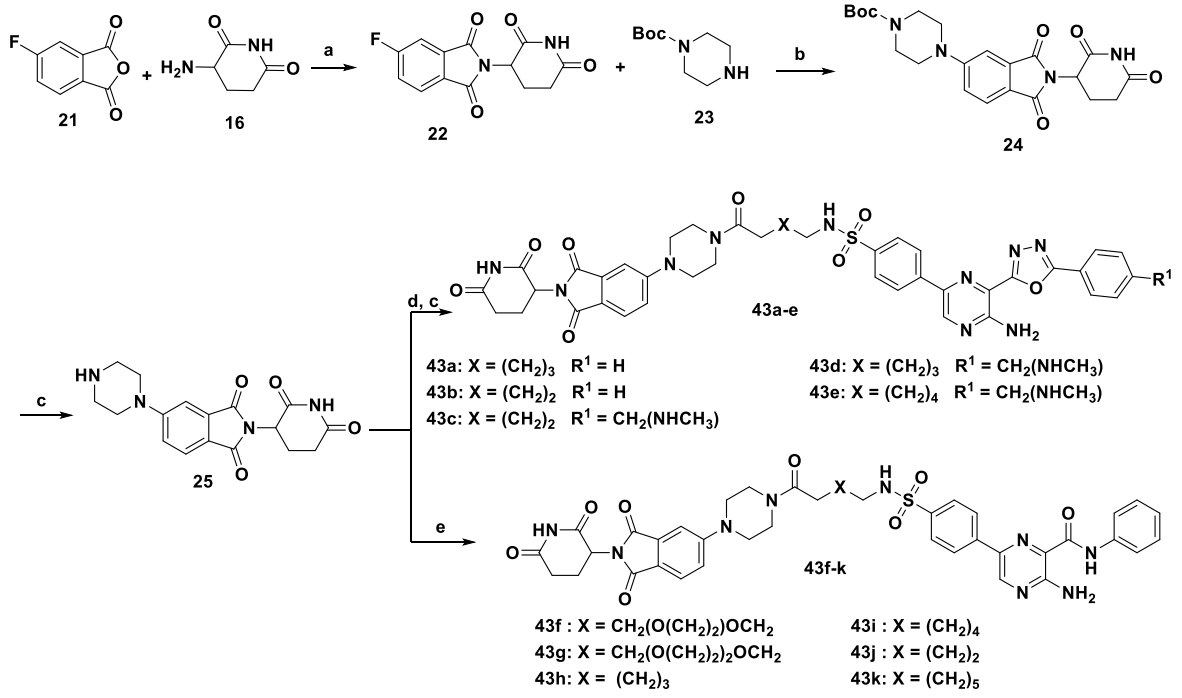

Scheme 3. Reagents and conditions: (a) AcOH, NaOAc (b) DIPEA, DMSO (c) DCM, TFA (d) **12a-e,** HATU, DIPEA, DMF (e) **13a-f**, HATU, DIPEA, DMF.

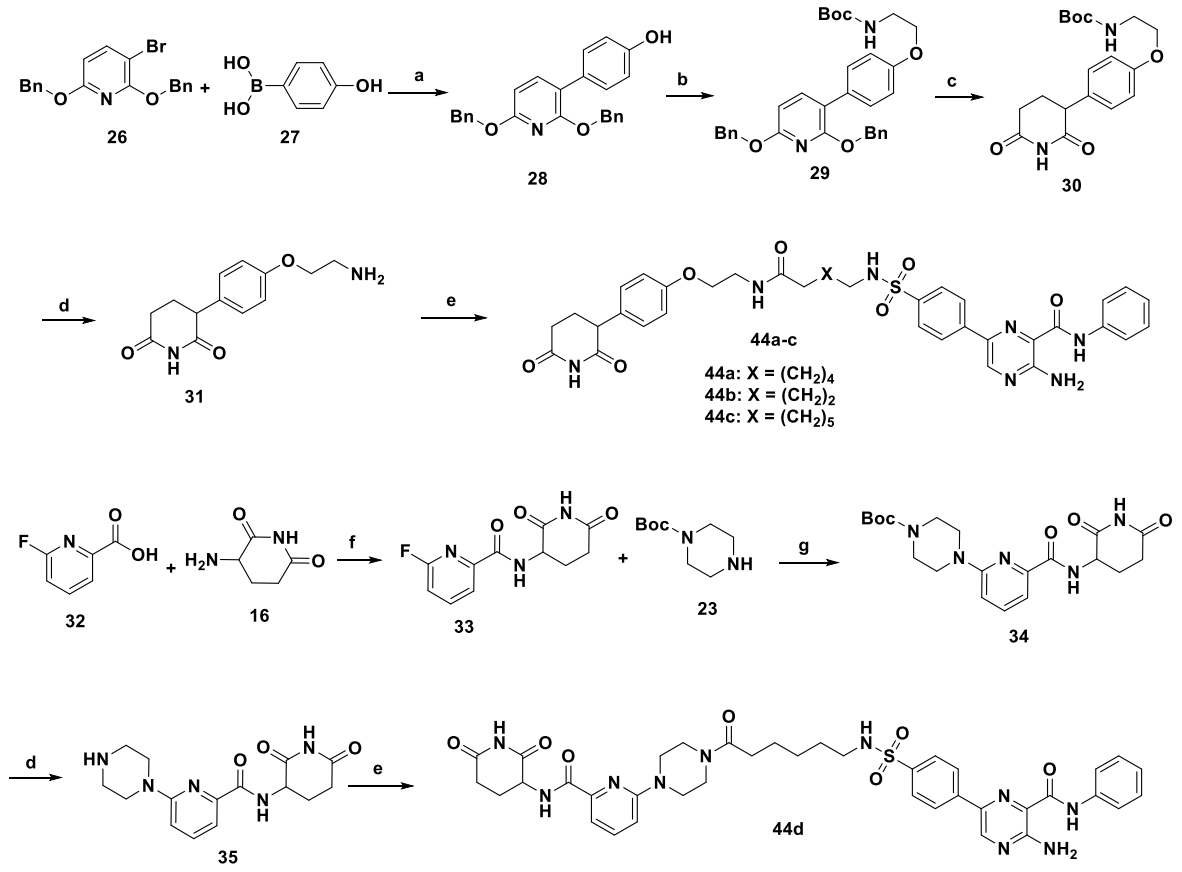

Scheme 4. Reagents and conditions: (a) $Pd(dppf)Cl_2$ Na_2CO_3, Dioxan, H_2O (b) Cs_2CO_3, *N*-Boc-2-bromoethyl amine (c) 10 % Pd/C, THF(d) DCM, TFA (e) **13a-f,** HATU, DIPEA, DMF (f) thionyl chloride, Acetonitrile, TEA (g) DIPEA, DMSO.

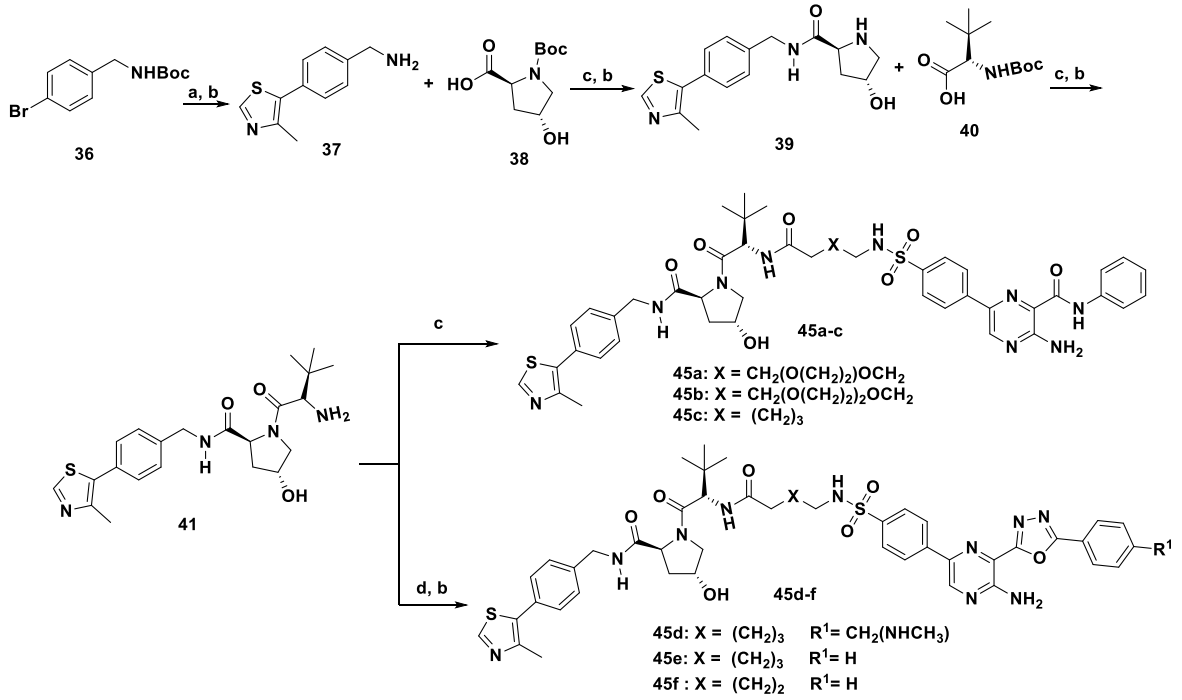

Scheme 5. Reagents and conditions: (a) 4-methylthiazole, $Pd(OAc)_2$, KOAc, DMF (b) DCM, TFA (c) **13a-f**, HATU, DIPEA, DMF (d) **12a-e**, HATU, DIPEA, DMF.

Table 1
Chemical structures of developed VHL-based PROTACs.

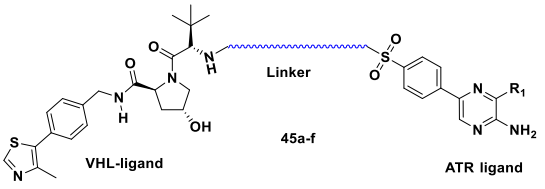

Cmpd. ID	Linker	R1
45a	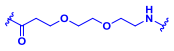	
45b	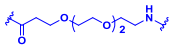	
45c	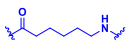	
45d	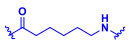	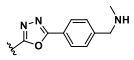
45e	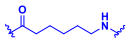	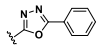
45f	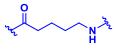	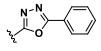

followed by Boc-deprotection to afford the picolinamide glutarimide derivative **35.**

Finally, The VHL-based PROTACs were synthesized using the VHL ligand **41** which has prepared following the previously reported procedures, as illustrated in Scheme 5 [33]. The *N*-Boc-4-bromobenzyl amine **36** was coupled with 4-methylthiazole, using the Heck coupling reaction followed by Boc-deprotection to afford the intermediate **37.** Then, the intermediate **37** was coupled with *N*-Boc-L-hydroxyprolin **38** and *N*-Boc-L-*tert*-leucine **40** respectively, through a HATU-mediated coupling reaction followed by Boc-deprotection after each coupling reaction afforded the corresponding VHL building block **41**.

The structures of the synthesized VHL-PROTACS and CRBN-PROTACS are outlined in Table 1 and Table 2, respectively.

2.3. Non-enzymatic stability testing

The reported CRBN-based PROTACs usually depend on the cereblon ligand thalidomide and its structurally related imide drugs (IMiDs) which are inherently unstable and readily undergoing hydrolysis in body fluids [34]. Also, it was found that IMiDs and IMiD-based PROTACs rapidly hydrolyze in PBS, and in relatively mild and widely utilized cell media [32]. Therefore, we tested the chemical stability of the synthesized PROTACs under cellular assay condition by using a non-enzymatic stability assay method. The selected CRBN-based PROTACs were dissolved in DMSO (10 μM) then diluted in the cellular assay media (Dulbecco's modified Eagle medium (DMEM) (50 %)/dimethyl sulfoxide (DMSO) (10 %)/acetonitrile (40 %)) and incubated at 37 °C for a maximum of 72 h. HPLC was used to determine the quantity of the compounds after 6, 12, 24, 48, and 72 h.

The results of the stability studies are presented in Table 3**.** It was founded that all tested compounds showed a relative high stability at cellular assay conditions over 72 h except for compound **43f**, which was only stable for 24h. Also, it was observed that lenalidomide and phenylglutarimide based PROTACs including the most active compound **42i** showed a high chemical stability profile without any degradation product after 72h. While the thalidomide based PROTACs showed moderate stability and showed two degradation products after 72h.

2.4. Plasma stability and protein binding

Plasma protein binding and plasma stability was measured for the CRBN-based PROTAC **42i** and the inhibitor **13g**. Plasma protein binding was found to be 77.5 ± 0.3 % for **13g** and 89.4 ± 0.3 % for the PROTAC **42i**. To determine the plasma stability the two compounds (20 μM, final DMSO concentration 1 %) were incubated at 37 °C and remaining amount was tested between 5 min and 24 h. The inhibitor **13g** showed high plasma stability (>90 %) over the 24-h period, while in the case of PROTAC **42i**, about 75 % of the original compound could still be detected after 24 h (Fig. 5, Tables S4 and S5 in the Supplement). The results show that the stability of CRBN-based PROTAC **42i** is also given in human plasma and that the compound can also be used for cellular and future in vivo studies.

2.5. ATR/ATRIP non-radioactive in vitro assay

To confirm the ATR inhibition of the developed PROTAC and the used inhibitor scaffold an in vitro assay was applied. In vitro testing of the PROTAC **42i** and the corresponding inhibitor **13g** was performed by Eurofins Discovery (Eurofins Discovery 11180 Roselle Street, Suite D, San Diego, CA 92121 USA) using the ATR/ATRIP complex and the KinaseProfiler™ assay. For the inhibitor **13g** an IC_{50} value of 1.0 ± 0.04 μM was measured. The PROTAC **42i** showed a weaker inhibition (IC_{50} > 10 μM). The IC_{50} plots are shown in Fig. S1 in the Supplement.

2.6. ATR degradation in cancer cells

We commenced our experiment with the screening of VHL-based, putative PROTACs in cellulo. The treatment of pancreatic cancer cells (MIA PaCa-2, isolated from the carcinoma of a 65-year-old male) with different doses of the VHL-based PRTOACs **45a-c** for 24 h yielded no reduction of ATR levels when compared to untreated cells. High doses (2 and 5 μM) of such PROTACs even increased ATR protein levels (Fig. 6a). Therefore, we did not test the remaining VHL-based PROTACs **45d-f** and focused on the testing of CRBN-based PROTACs. Such lenalidomide-based PROTACs could attenuate ATR expression. 500 nM of **42i** (based on the ATR inhibitor **VE-821**) reduced ATR to 40 % of its levels in untreated cells. To study the optimal linker length, we tested **42j** and **42k.** These compounds harbor longer or shorter linkers, respectively, than **42i**. One μM **42j** produced similar ATR-reducing effects as **42i** but failed to attenuate the expression of ATR in its active form, i.e., phosphorylated at the T1989 residue. **42j** even augmented this post-translational modification of ATR. Compound **42k** was less active than **42i**. Treatment with 2 μM **42h** could decrease ATR levels by 50 %. **42l** proved to be less effective than such compounds (Fig. 6b). We additionally tested lenalidomide-based PROTACs that contain VE-822 and **II** as ATR inhibitors. 40 % reduction in ATR levels was achievable with 2 μM **42a** and **42c**. Very weak effects on ATR expression levels (not exceeding 20 % reduction) were observed with **42e-g**. Only a slight increase in ATR levels was noted with **42b** and **42d** (Fig. 6c).

Different doses of the thalidomide- and **VE-821**-based PROTACs **43f, 43g, 43j,** and **43k** either had no effects on ATR levels or even raised its expression. Of such PROTACs, 5 μM **43h** reduced ATR to 40 % of its levels in untreated cells, but a minor lessening effect was noted upon **43i** treatment (Fig. 6d). Considering the thalidomide-based PROTACs **43b, 43c,** and **43e**, that harbor scaffold **IIb** as ATR inhibitor moiety, weak attenuation of ATR expression was observed. Immunoblot analyses revealed that **43a** and **43d** induced higher ATR expression levels than those in control cells (Fig. 6e). We expanded our study to include PROTACs based on other glutarimide moieties exemplified by **44a** and **44b**, which could not reduce ATR levels reproducibly, as well as **44c** and **44d**, which augmented the ATR protein levels (Fig. 6f). Thus, our biological screening positions **42i** as the most promising compound.

We pursued other experiments with **42i** as it was the most potent and dose-dependent ATR degrader in our screen. To ascertain that the impact of **42i** on ATR is not just a consequence of cell death, we used the

Table 2
Chemical structures of developed CRBN-based PROTACs.

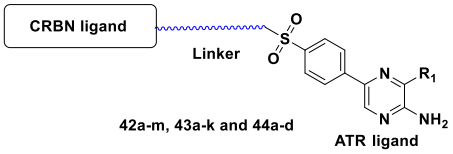

Cmpd. ID	CRBN ligand	Linker	R1
42a	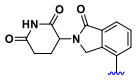	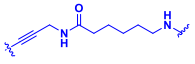	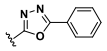
42b	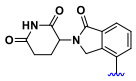	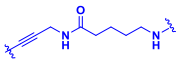	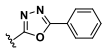
42c	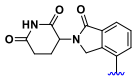	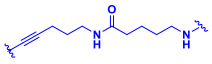	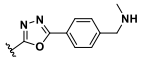
42d	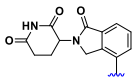	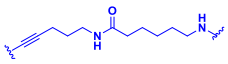	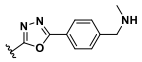
42e	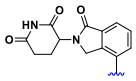	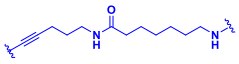	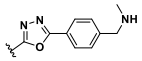
42f	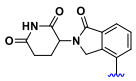	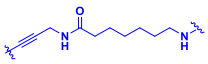	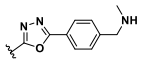
42g	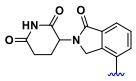	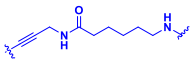	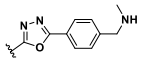
42h	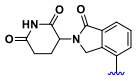	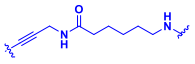	
42i	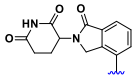	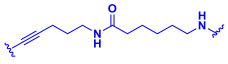	
42j	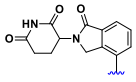	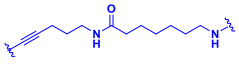	
42k	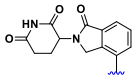	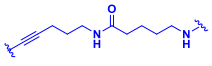	
42l	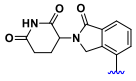	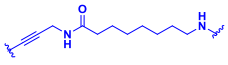	
42m (negative control)	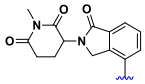	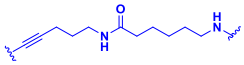	

(*continued on next page*)

Table 2 (*continued*)

Cmpd. ID	CRBN ligand	Linker	R1
43a	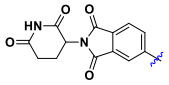	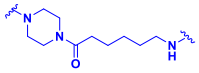	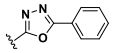
43b	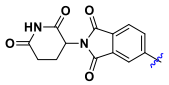	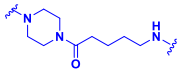	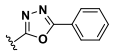
43c	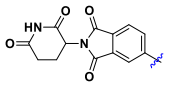	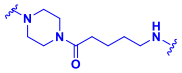	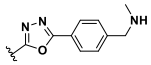
43d	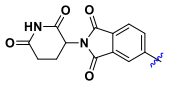	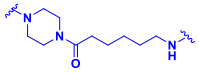	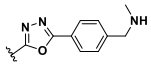
43e	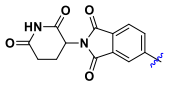	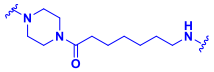	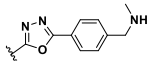
43f	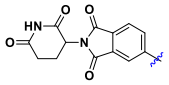	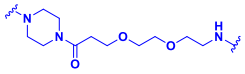	
43g	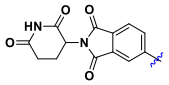	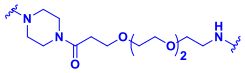	
43h	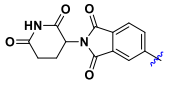	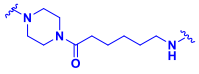	
43i	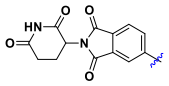	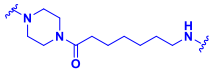	
43j	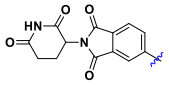	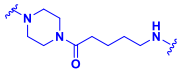	
43k	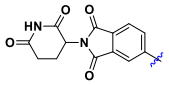	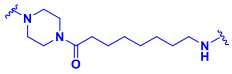	
44a	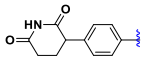	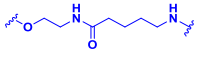	
44b	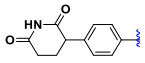	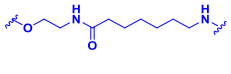	
44c	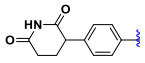		
44d			

very sensitive flow cytometry-based annexin-V/propidium iodine (PI) staining [35]. We found that **42i** did not compromise cell vitality, illustrating that the loss of ATR that this new agent induces is a direct effect (Fig. 6g).

A key property of an ATR PROTAC is specificity for this apical checkpoint kinase. To investigate the effects of **42i** on the structurally and functionally ATR-related checkpoint kinases ATM and DNA-PKcs protein levels upon treatment of MIA PaCa-2 cells with different doses

Table 3
Stability of PROTACs and inhibitors in assay medium at 37 °C.

Cpd. ID	Class	0h - %	6h - %	12h - %	24h - %	48h - %	72h - %
42a	PROTAC ATR-CRBN	100	108	105	105	106	106
42b	PROTAC ATR-CRBN	100	104	105	105	103	107
42c	PROTAC ATR-CRBN	100	101	101	102	100	100
42d	PROTAC ATR-CRBN	100	104	103	103	103	102
42e	PROTAC ATR-CRBN	100	101	101	101	95	93
42f	PROTAC ATR-CRBN	100	101	101	101	100	101
42g	PROTAC ATR-CRBN	100	101	101	101	100	100
42h	PROTAC ATR-CRBN	100	101	103	104	105	109
42i	PROTAC ATR-CRBN	100	102	104	106	110	115
42j	PROTAC ATR-CRBN	100	102	103	105	105	109
42k	PROTAC ATR-CRBN	100	102	102	102	103	103
42l	PROTAC ATR-CRBN	100	100	100	98	77	47
43a	PROTAC ATR-CRBN	100	96	92	90	80	73
43b	PROTAC ATR-CRBN	100	99	95	91	85	77
43c	PROTAC ATR-CRBN	100	97	99	91	83	74
43d	PROTAC ATR-CRBN	100	98	95	92	81	71
43e	PROTAC ATR-CRBN	100	97	95	91	79	72
43f	PROTAC ATR-CRBN	100	100	95	80	21	6
43g	PROTAC ATR-CRBN	100	101	100	97	83	74
43h	PROTAC ATR-CRBN	100	101	101	96	87	72
43i	PROTAC ATR-CRBN	100	97	92	88	78	70
43j	PROTAC ATR-CRBN	100	97	94	90	82	74
43k	PROTAC ATR-CRBN	100	98	105	108	94	84
44a	PROTAC ATR-CRBN	100	101	103	102	102	101
44b	PROTAC ATR-CRBN	100	101	101	101	99	99
44c	PROTAC ATR-CRBN	100	100	99	100	100	100
44d	PROTAC ATR-CRBN	100	102	104	97	82	65
45a	PROTAC-ATR-VHL	100	100	100	101	101	102
45b	PROTAC-ATR-VHL	100	100	100	102	103	105
45c	PROTAC-ATR-VHL	100	99	99	100	100	100
45d	PROTAC-ATR-VHL	100	101	100	101	99	99
45e	PROTAC-ATR-VHL	100	100	100	102	103	104
45f	PROTAC-ATR-VHL	100	100	100	102	103	104
42m	negative control	100	100	100	99	98	97
13g	ATR Inhibitor	100	99	100	100	102	104

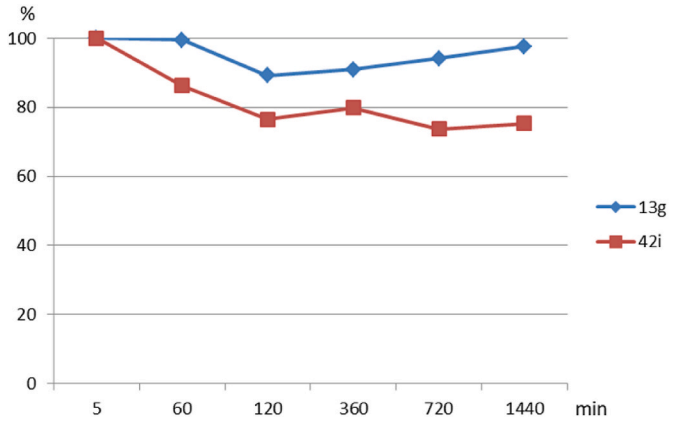

Fig. 5. Plasma stability of PROTAC **42i** and the inhibitor **13g** measured for 24h.

of **42i**. The levels of these apical checkpoint kinases as well as the expression of the pro-proliferative CRBN neosubstrate GSPT1 did not change in **42i** treated cancer cells (Fig. 7a). To verify our results in an independent cell system, we used cervix carcinoma cells (HeLa, from a 31-year-old female). In these cells, we noted a degradation of ATR and *p*-ATR by 60–70 % upon treatment with 500 nM **42i**. The ATR-related proteins ATM and DNA-PKcs were not attenuated by **42i** (Fig. 7b). These data show that **42i** decreases ATR and *p*-ATR levels without affecting related checkpoint kinases in male and female tumor cells from different anatomical sites.

To verify the anticipated proteasomal ATR degradation, we pre-incubated MIA PaCa-2 cells with two structurally different proteasome inhibitors, bortezomib (50 nM) and MG132 (10 μM), and then treated the cells with 2 μM **42i** for 3 h. We chose this shorter time point to avoid the detection of processes that are related to proliferation arrest and cell death upon proteasome inhibition. Both proteasome inhibitors rescued the **42i** mediated ATR degradation (Fig. 7c), verifying that **42i** accelerates the proteasomal degradation of ATR. We confirmed the on-target activity of both proteasome inhibitor by immunoblot for poly-ubiquitin which can be revealed as smear of high molecular weight proteins accumulating upon inactivated proteasomes (Fig. 7c).

To corroborate that **42i** is an ATR degrader, we treated MIA PaCa-2 cells with the ATR inhibitor **VE-821** on which our PROTAC is based. **VE-821** failed to decrease ATR expression. Consistent with the above findings, **42i** significantly reduced ATR levels by 40 % (Fig. 7d). Hence, the ATR PROTAC **42i** has functional properties superseding its parental compound. To further corroborate the functionality of CRBN for the **42i** induced ATR degradation, we designed the **42i** derived negative control **42m**. This molecule cannot bind CRBN due to methylated glutarimide moiety. **42m** failed to reduce ATR level as a single treatment of MIA PaCa-2 cells (Fig. 7d).

Next, we asked if **42i** could reduce ATR that was activated upon DNA replication stress. Combinatorial treatment of cancer cells with the topoisomerase I inhibitor irinotecan (5 μM), which is clinically used to treat PDAC [24], and **42i** attenuated the ATR levels by 80 % relative to single chemotherapeutic treatment regimen. Irinotecan induced high expression levels of both *p*-ATR (T1989) and its direct downstream target *p*-CHK1 (S345). **42i** reduced their levels up to 0.1- and 0.5-fold, respectively (Fig. 7e).

Due to its lenalidomide part, **42i** is expected to decrease ATR through a CRBN-containing E3 ubiquitin ligase complex. We aimed to prove this with a genetic approach using RNAi. A transient knock-down of CRBN consolidated the anticipated ATR degradation by **42i**. Treatment of MIA PaCa-2 cells with siRNA against CRBN halted the PROTAC-mediated depletion of ATR, *p*-ATR, and *p*-CHK1 expression levels. Irinotecan and **42i** did not alter CRBN expression (Fig. 7e).

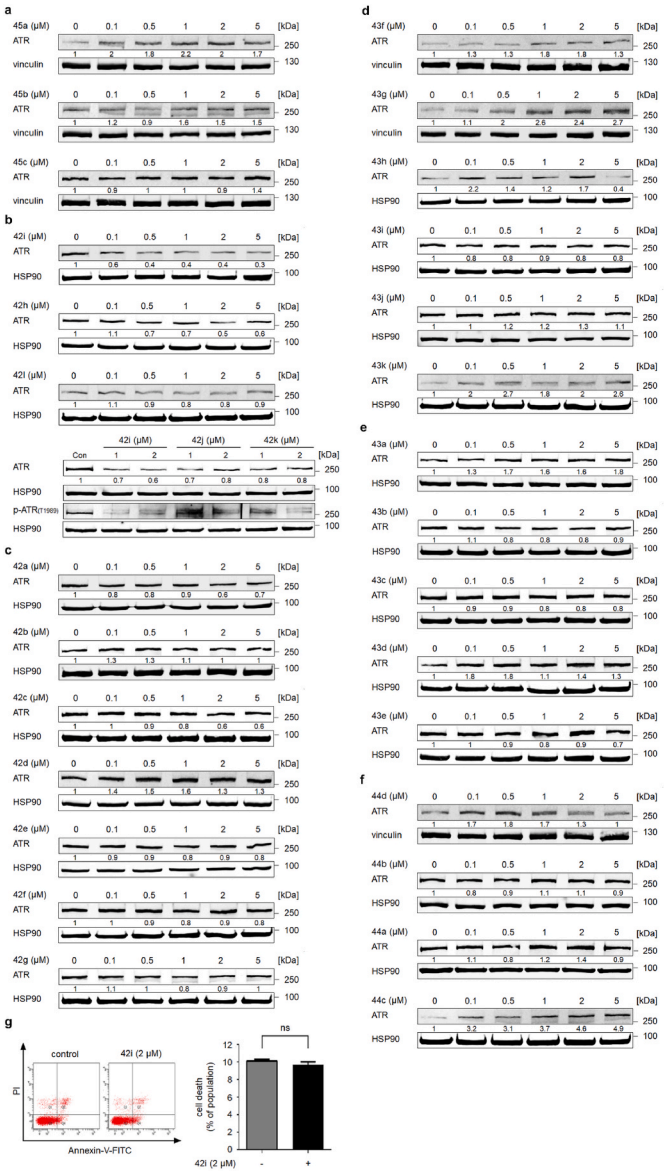

Fig. 6. Screening of potential ATR-PROTACs in cancer cells. (a) Lysates from MIA PaCa-2 cells that were treated with the VHL-based PROTACs **45a**, **45b**, and **45c** (0.1, 0.5, 1, 2, and 5 μM) for 24 h were subjected to immunoblot analyses. The immunoblots show ATR; vinculin serves as independent loading control for each membrane. (b) Lysates from MIA PaCa-2 cells that were treated with the lenalidomide- and VE-821-based PROTACs **42i**, **42h**, **42l** (0.1, 0.5, 1, 2, and 5 μM), **42j**, and **42k** (1 and 2 μM) for 24 h were subjected to immunoblot analyses. The immunoblots show ATR and *p*-ATR (T1989); HSP90 serves as independent loading control for each membrane. (c) Lysates from MIA PaCa-2 cells that were treated with the lenalidomide- and other ATR inhibitor-based PROTACs **42a**, **42b**, **42c**, **42d**, **42e**, **42f**, and **42g** (0.1, 0.5, 1, 2, and 5 μM) for 24 h were subjected to immunoblot analyses. The immunoblots show ATR; HSP90 serves as independent loading control for each membrane. (d) Lysates from MIA PaCa-2 cells that were treated with the thalidomide- and VE-821-based PROTACs **43f**, **43g**, **43h**, **43i**, **43j**, and **43k** (0.1, 0.5, 1, 2, and 5 μM) for 24 h were subjected to immunoblot analyses. The immunoblots show ATR; HSP90 and vinculin serve as independent loading controls for each membrane. (e) Lysates from MIA PaCa-2 cells that were treated with the thalidomide- and other ATR inhibitor-based PROTACs **43a**, **43b**, **43c**, **43d**, and **43e** (0.1, 0.5, 1, 2, and 5 μM) for 24 h were subjected to immunoblot analyses. The immunoblots show ATR; HSP90 serves as independent loading control for each membrane. (f) Lysates from MIA PaCa-2 cells that were treated with other glutarimide-based PROTACs **44a**, **44b**, **44c**, and **44d** (0.1, 0.5, 1, 2, and 5 μM) for 24 h were subjected to immunoblot analyses. The immunoblots show ATR; HSP90 and vinculin serve as independent loading controls for each membrane. Numbers below the respective proteins indicate densitometric values of the protein expression levels, normalized to the loading controls; protein levels of untreated cells were defined as 1.0 (n = 2 ± SD). (g) Representative flow cytometry dot plots and dose-response chart of MIA PaCa-2 cells that were treated with **42i** (2 μM) for 24 h. Cells were stained with annexin-V/PI and measured via flow cytometry for the induction of cell death (n = 3 ± SD; Student's t-test; ns "non-significant").

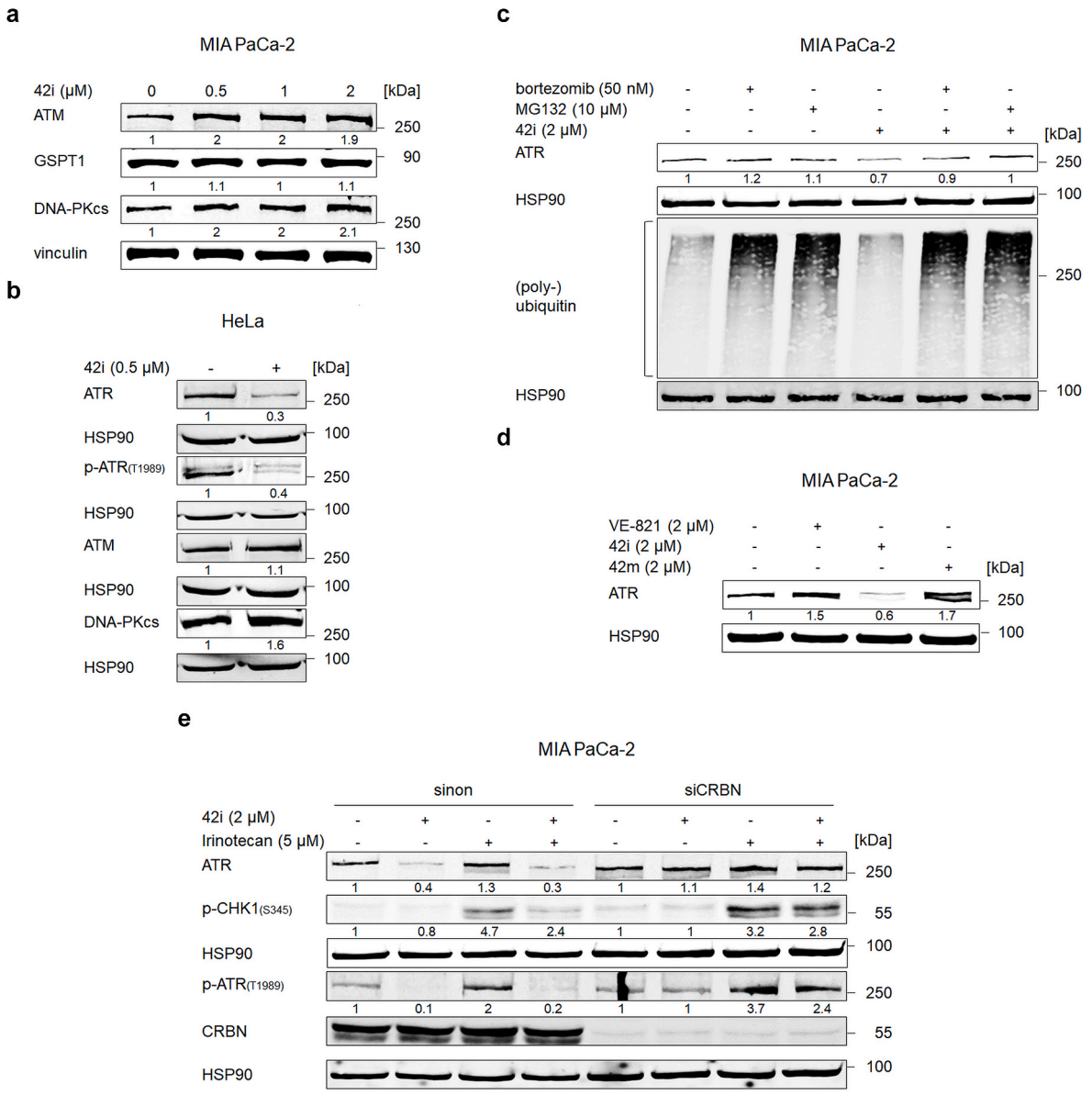

Fig. 7. Specificity of the ATR-PROTAC **42i** in cancer cells. (a) Lysates from MIA PaCa-2 cells that were treated with **42i** (0.5, 1, and 2 μM) for 24 h were subjected to immunoblot analyses. The immunoblots show ATM, GSPT1, and DNA-PKcs; vinculin serves as independent loading control for each membrane. (b) Lysates from HeLa cells that were treated with **42i** (0.5 μM) for 24 h were subjected to immunoblot analyses. The immunoblots show ATR, *p*-ATR (T1989), ATM, and DNA-PKcs. HSP90 serves as loading control for each membrane. (c) Lysates from MIA PaCa-2 cells that were treated with **42i** (2 μM) for 3 h and/or bortezomib (50 nM) or MG132 (10 μM) for 4 h were subjected to immunoblot analyses. The immunoblots show ATR and ubiquitin; HSP90 serves as independent loading control for each membrane. (d) Lysates from MIA PaCa-2 cells that were treated with the ATR inhibitor VE-821 (2 μM), **42i** (2 μM), and **42m** (2 μM) for 24 h were subjected to immunoblot analysis. The immunoblot shows ATR; HSP90 serves as loading control for the membrane. (e) Lysates from MIA PaCa-2 cells (with and without CRBN knockdown by RNAi) that were treated with **42i** (2 μM) and/or irinotecan (5 μM) for 24 h. The immunoblots show ATR, *p*-CHK1 (S345), *p*-ATR (T1989), and CRBN; HSP90 serves as independent loading control for each membrane; sinon, non-targeting control siRNA. Numbers below the respective proteins indicate densitometric values of the protein expression levels, normalized to the loading controls; protein levels of untreated cells were defined as 1.0 (n = 2 ± SD).

2.7. Cytotoxicity of developed PROTACs and inhibitors against HEK239 cells

To evaluate the potential toxicity of our most active ATR PROTAC on human embryonic kidney cell line (HEK293), we did cytotoxicity test for all synthesized PROTACs and inhibitors (Table 4). Only PROTACs **45a** and **45b** showed a decreased cell viability at 50 μM concentration after 24h. The inhibitor **13g** as well as the active PRTOAC **42i** did not produce cytotoxic effects against HEK293 cells at a high concentration (50 μM).

3. Conclusion

We present the first-in-class ATR-targeting PROTACs. These are based on three potent and selective ATR inhibitors with a 3-aminopyrazine scaffold. Of these agents, the lenalidomide (CRBN ligand)-based PROTAC **42i** exhibits the highest ATR degradation potential in tumor cells. **42i** selectively decreases ATR and phospho-ATR without affecting the related apical checkpoint kinases ATM and DNA-PKcs. In addition, proteasome inhibitors as well as knock-down of CRBN prevent the **42i** mediated depletion of ATR, emphasizing that **42i** induces ATR degradation through the ubiquitin-proteasome-system. In addition, **42i** attenuates the activated ATR signalling pathway efficiently in cells with

Table 4
Cytotoxicity against HEK293 cells at 50 μM inhibitor concentration after 24 h treatment. (n = 3 ± SD).

Cpd. ID	Cell viability (%)	SD (%)	Cpd. ID	Cell viability (%)	SD (%)
42a	70.5	5.3	**43f**	79.9	1.5
42b	95.5	5.1	**43g**	75.0	5.2
42c	107.3	3.4	**43h**	96.0	3.3
42d	101.4	7.4	**43i**	93.2	4.8
42e	91.8	4.6	**43j**	102.4	4.6
42f	89.5	1.5	**43k**	90.5	1.7
42g	101.6	4.4	**44a**	95.7	4.7
42h	86.4	4.2	**44b**	66.4	5.4
42i	77.1	4.2	**44c**	62.9	5.9
42j	109.3	2.9	**44d**	86.5	3.5
42k	103.6	2.3	**45a**	44.5	0.6
42l	94.2	1.4	**45b**	45.7	4.0
42m	83.5	5.3	**45c**	60.3	2.8
43a	85.6	2.5	**45d**	81.8	1.6
43b	97.6	0.7	**45e**	79.8	3.4
43c	103.7	5.2	**45f**	91.1	5.3
43d	105.4	1.4	**13g**	83.7	6.7
43e	95.7	4.4	**medium**	100.0	3.0

replication stress. In summary, these results suggest that **42i** is a promising candidate for further optimization and biological characterization as inducers of ATR degradation through proteasomes.

4. Experimental section

4.1. General

All materials and reagents were purchased from Sigma Aldrich Co. Ltd. and abcr GmbH and used without further purification. All solvents were analytically pure and were dried before use. All reactions were monitored by TLC (Kieselgel 60 F254 pre-coated plates, E. Merck, Darmstadt, Germany); the spots were detected by UV lamp at λ 254 nm. For medium-pressure liquid chromatography (MPLC), Biotage SNAP ultra-HP-sphere 25 μm columns containing silica gel were used. Dichloromethane: methanol and n-heptane: Ethyl acetate were used as elution systems for MPLC. In the preparative high-pressure liquid chromatography used for purification of several PROTACs, LiChrosorb® RP-18 (7 μm) 250-25 Merck (Merck, Darmstadt, Germany) column was used. The applied mobile phase was a gradient with increasing polarity composed of acetonitrile/water/formic acid. Purity was determined using HPLC by measuring the UV absorbance at 254 nm. The HPLC consisted of a LiChrosorb® RP-18 (5 μm) 100–4.6 Merck column (Merck, Darmstadt, Germany), two LC-10AD pumps, a SPD-M10A VP PDA detector, and a SIL-HT autosampler, all from the manufacturer Shimadzu (Kyoto, Japan). The absorption spectra were recorded with a SPD-M10A diode array detector Shimadzu spectrophotometer (Kyoto, Japan). Mass spectrometry analyses were performed with a Finnigan MAT710C (Thermo Separation Products, SanJose, CA, USA) for the ESI MS spectra and with a LTQ (linear ion trap) Orbitrap XL hybrid mass spectrometer (Thermo Fisher Scientific, Bremen, Germany) for the HRMS-ESI (high-resolution mass spectrometry) spectra. ^{1}H NMR and ^{13}C NMR spectra were taken on a Varian Inova 400 using deuterated dimethyl sulfoxide (DMSO-d_6) or deuterated chloroform ($CDCl_3$) as solvent. Chemical shifts were referenced to the residual solvent signals. The following abbreviations and formulas for solvents and reagents were used: ethyl acetate (EtOAc), N,N-dimethylformamide (DMF), dimethyl sulfoxide (DMSO), tetrahydrofuran (THF), triethylamine (TEA), water (H_2O), dichloromethane (DCM), N,N-diisopropylethylamine (DIPEA), O-(7-azabenzotriazol-1-yl)-*N*,*N*,*N*′,*N*′-tetramethyluronium-hexafluorphosphate (HATU), Triphenylphosphine (PPh_3), bis(pinacolato)diboron (B_2pin_2), (1,1′-Bis(diphenylphosphino)ferrocene)palladium(II) dichloride (Pd(dppf)Cl_2) and trifluoroacetic acid (TFA).

4.2. General synthetic methods

4.2.1. Method I: reaction of amine and acid chloride

Method I-A: To a stirred solution of the appropriate amine (1.0 equiv.) and triethylamine (3 equiv.) in acetonitrile at 0 °C, acid chloride (1.05 equiv.) was added. Then, the reaction mixture was allowed to stir at room temperature for 4–7 h. After completion of the reaction as indicated by TLC, the reaction was quenched with 5 % acetic acid solution and extracted with ethyl acetate. The combined organic layer was washed with brine and dried over anhydrous sodium sulfate, then the solvent was evaporated under reduced pressure to yield the crude amide, which was purified by the MPLC using n-heptane/ethyl acetate or MeOH/DCM.

Method I–B: To a stirred solution methyl amine hydrochloride (1.0 equiv.) and sodium bicarbonate (3 equiv.) in Ethyl acetate:H_2O (1:1) (50 mL), 4-bromobenzensulfonyl chloride (0.5 equiv.) was added portion-wise. Then, the reaction mixture was allowed to stir at room temperature for overnight. After completion of the reaction as indicated by TLC, the organic layer was separated, washed with brine, and dried over anhydrous sodium sulfate, and then the solvent was evaporated under reduced pressure to yield the corresponding 4-bromobenzene sulfonamide derivative.

4.2.2. Method II: hydrolysis of methyl ester

To a stirred solution of the appropriate methyl ester (1.0 equiv.) in THF:H_2O (3:1), LiOH.H_2O (5.0 equiv.) was added, and the mixture was stirred at room temperature for 4–6 h. After complete ester hydrolysis, 1 M hydrochloric acid solution was added dropwise to the reaction to liberate the free acid, which was extracted with ethyl acetate. The combined organic layer was washed with brine and dried over anhydrous sodium sulfate, and then the solvent was evaporated under reduced pressure to give the corresponding carboxylic acid.

4.2.3. Method III: hydrolysis of tert-butyl ester

The *tert*-butyl ester was dissolved or suspended in DCM at 0 °C (5 mL), and then trifluoroacetic acid (5 mL) was added dropwise. The reaction mixture was stirred at room temperature for 3–4 h. After complete ester hydrolysis, the solvent was evaporated to dryness to provide the corresponding carboxylic acid.

4.2.4. Method IV: amide coupling

A solution of the appropriate carboxylic acid (1.0 equiv.) and HATU (1.1 equiv.) in DMF was stirred at room temperature for 30 min, then the corresponding amine derivative (1.0 equiv.) and DIPEA (4.0 equiv.) were added. The reaction mixture was stirred at room temperature for 4–6 h. After completion of the reaction as indicated by TLC, the reaction was quenched with 1 M ammonium chloride solution and extracted with ethyl acetate. The organic layer was washed with an aqueous 1 M sodium bicarbonate solution and brine. The combined organic layer was dried over anhydrous sodium sulfate, and then the solvent was evaporated under reduced pressure to yield the crude amide, which was purified by the MPLC using n-heptane/ethyl acetate or MeOH/DCM.

4.2.5. Method V: Miyaura borylation

A solution of bromoaryl derivative (1 equiv.), bis(pinacolato)diboron (1.2 equiv.), potassium acetate (3 equiv.), and Pd(dppf)Cl_2 (0.1 equiv.) in dioxan was degassed and flushed with argon three times, and then heated at 80 °C for 6–8 h. The reaction mixture was cooled to room temperature, diluted with ethyl acetate, and filtered through Celite. The filtrate was evaporated under reduced pressure to yield the crude product, which was purified by the MPLC using n-heptane/ethyl acetate or MeOH/DCM.

4.2.6. Method VI: Suzuki coupling

A solution of bromoaryl derivative (1 equiv.), the appropriate boronic derivative (1 equiv.), Na_2CO_3 (4 equiv.), and Pd(dppf)Cl_2 (0.1

equiv.) in 25 ml dioxan:H_2O (5:1) was degassed and purged with argon three times. The reaction mixture was heated at 90 °C for 6–8 h. The reaction mixture was cooled to room temperature, diluted with ethyl acetate, and filtered through Celite. The filtrate was evaporated under reduced pressure, and the residue was purified by MPLC using n-heptane/ethyl acetate.

4.2.7. Method VII: Boc-deprotection

Method VII-A: To a stirred solution or suspension of Boc-protected amine in DCM (5 mL) at 0 °C, trifluoroacetic acid (5 mL) was added dropwise, and the solution was stirred at room temperature for 1 h. After completion of the reaction, the mixture was evaporated under reduced pressure to afford the crude product as trifluoroacetate salt, which can be directly used in the next step without further purification.

Method VII-B: To a stirred solution of Boc-protected amine and 1,2-ethanedithiol (0.5 mL) in DCM (5 mL) at 0 °C, trifluoroacetic acid (5 mL) was added dropwise and the solution was stirred at room temperature for 1 h. After completion of the reaction, the mixture was evaporated under reduced pressure. After that, the residue was dissolved again in DCM, neutralized with triethyl amine and evaporated under reduced pressure to yield the crude product, which was purified by the MPLC or preparative HPLC.

4.2.8. Method VIII: Alkylation reaction

To a stirred solution of compound (**5, 17a** or **28** (1.0 equiv.)) and a base (K_2CO_3, Cs_2CO_3 or NaH (2.5 equiv.)) in 25 ml of DMF, an appropriate alkyl halide (2 equiv.) was added, and the solution was stirred at room temperature overnight. The mixture was diluted with 60 mL of water and extracted with ethyl acetate three times. The combined organic layers were washed with brine, dried over Na_2SO_4, and evaporated under reduced pressure to yield the crude product, which was purified by the MPLC using n-heptane/ethyl acetate or MeOH/DCM.

4.2.9. Method IX: hydrogenation

To a stirred solution of compound **29** in THF (20 mL), a catalytic amount of Pd/C (10 %) was added under an inert atmosphere, then the reaction mixture was stirred overnight under a hydrogen atmosphere at room temperature. The reaction mixture was filtered through a short pad of Celite, washed with ethyl acetate and concentrated to dryness. The crude product was purified by the MPLC using n-heptane/ethyl acetate.

4.2.10. Method X: synthesis of 1,3,4-oxadiazole

To a stirred mixture of pyrazine carboxylic acid **9** (1.0 equiv.), the appropriate benzohydrazide derivative (1.0 equiv.), tetrabromoethane (2.5 equiv.) and TEA (3.0 equiv.) in DCM (25 mL) at 0 °C, triphenylphosphine (2.5 equiv.) was added portion wise over 10 min, and the reaction was then stirred at room temperature for 2 h. After that the mixture was evaporated under reduced pressure and the residue was purified by MPLC using n-heptane/ethyl acetate.

4.2.11. Method XI: reaction of piperazine with fluoroaromatic compounds

To a stirred solution of fluoroaromatic compound (1.0 equiv.) and DIPEA (3.0 equiv.) in DMSO (25 mL), 1-Boc-piperazine (1.1 equiv.) was added and the reaction was then heated at 130 °C for 4–5 h. After completion of the reaction, the reaction was quenched with 5 % acetic acid solution and extracted with ethyl acetate. The combined organic layer was washed with brine and dried over anhydrous sodium sulfate, then the solvent was evaporated under reduced pressure to yield the crude product, which was purified by the MPLC using n-heptane/ethyl acetate.

4.3. Characterization data of key intermediates and final compounds

The preparation and analytical data of Intermediates **9**, **11a** [8], **20a-c** [30], **25** [31], **28** [32] and **41** [33] were as reported.

4.3.1. Synthesis and characterization of intermediates 3a-g and 4a-d

The 4-bromobenzensulfonyl chloride reacted with alkyl and PEG linkers **1a-f** according to method I-A and also reacted with methyl amine hydrochloride **1g** according to method I–B to give the corresponding 4-bromobenzenesulphonamide derivatives **3a-g**. Then the intermediates **3a-d** were further converted to the corresponding boronates **4a-d** according to method V.

Methyl 5-((4-bromophenyl)sulfonamido)pentanoate (3a). ^{1}H NMR (400 MHz, $CDCl_3$) δ 7.74–7.68 (m, 2H), 7.66–7.61 (m, 2H), 5.04 (t, J = 6.0 Hz, 1H), 3.63 (s, 3H), 2.93 (q, J = 6.6 Hz, 2H), 2.26 (t, J = 7.1 Hz, 2H), 1.65–1.44 (m, 4H).

Methyl 6-((4-bromophenyl)sulfonamido)hexanoate (3b). ^{1}H NMR (400 MHz, $CDCl_3$) δ 7.74–7.69 (m, 2H), 7.66–7.61 (m, 2H), 4.91 (t, J = 6.1 Hz, 1H), 3.64 (s, 3H), 2.93 (dd, J = 13.3, 6.9 Hz, 2H), 2.25 (t, J = 7.4 Hz, 2H), 1.61–1.41 (m, 4H), 1.35–1.22 (m, 2H).

Methyl 7-((4-bromophenyl)sulfonamido)heptanoate (3c). ^{1}H NMR (400 MHz, $CDCl_3$) δ 7.74–7.69 (m, 2H), 7.67–7.61 (m, 2H), 4.86 (t, J = 5.1 Hz, 1H), 3.64 (s, 3H), 2.92 (dd, J = 13.3, 6.9 Hz, 2H), 2.26 (t, J = 7.4 Hz, 2H), 1.60–1.40 (m, 4H), 1.33–1.17 (m, 4H).

Methyl 8-((4-bromophenyl)sulfonamido)octanoate (3d). ^{1}H NMR (400 MHz, $CDCl_3$) δ 7.75–7.68 (m, 2H), 7.66–7.60 (m, 2H), 4.93 (t, J = 5.8 Hz, 1H), 3.64 (s, 3H), 2.91 (dd, J = 13.3, 6.9 Hz, 2H), 2.26 (t, J = 7.5 Hz, 2H), 1.62–1.37 (m, 4H), 1.30–1.15 (m, 6H).

***Tert*-butyl 3-(2-(2-((4-bromophenyl)sulfonamido)ethoxy)ethoxy)propanoate** (3e). ^{1}H NMR (400 MHz, $CDCl_3$) δ 7.77–7.69 (m, 2H), 7.67–7.59 (m, 2H), 5.45 (t, J = 5.7 Hz, 1H), 3.69 (t, J = 6.3 Hz, 2H), 3.59–3.41 (m, 6H), 3.11 (dd, J = 10.4, 5.5 Hz, 2H), 2.49 (t, J = 6.4 Hz, 2H), 1.43 (s, 9H).

***Tert*-butyl 3-(2-(2-(2-((4-bromophenyl)sulfonamido)ethoxy)ethoxy)ethoxy)propanoate (3f).** ^{1}H NMR (400 MHz, $CDCl_3$) δ 7.77–7.68 (m, 2H), 7.67–7.58 (m, 2H), 5.48 (t, J = 5.8 Hz, 1H), 3.69 (t, J = 6.5 Hz, 2H), 3.64–3.43 (m, 10H), 3.11 (dd, J = 10.4, 5.7 Hz, 2H), 2.48 (t, J = 6.5 Hz, 2H), 1.42 (s, 9H).

4-bromo-N-methylbenzenesulfonamide (3g) ^{1}H NMR (400 MHz, $CDCl_3$) δ 7.75–7.70 (m, 2H), 7.68–7.62 (m, 2H), 4.79 (m, 1H), 2.65 (d, J = 5.3 Hz, 3H).

Methyl 5-((4-(4,4,5,5-tetramethyl-1,3,2-dioxaborolan-2-yl)phenyl)sulfonamido)pentan-oate (4a). *m/z* ($APCI^+$) 398.2 (M + H). ^{1}H NMR (400 MHz, $CDCl_3$) δ 7.92 (d, J = 8.3 Hz, 2H), 7.82 (d, J = 8.3 Hz, 2H), 4.78 (t, J = 6.2 Hz, 1H), 3.62 (s, 3H), 2.92 (q, J = 6.7 Hz, 2H), 2.25 (t, J = 7.1 Hz, 2H), 1.64–1.43 (m, 4H), 1.34 (s, 12H).

Methyl 6-((4-(4,4,5,5-tetramethyl-1,3,2-dioxaborolan-2-yl)phenyl)sulfonamido)hexan-oate (4b). *m/z* ($APCI^+$) 412.3 (M + H). ^{1}H NMR (400 MHz, $CDCl_3$) δ 7.92 (d, J = 8.3 Hz, 2H), 7.83 (d, J = 8.3 Hz, 2H), 4.67 (t, J = 6.2 Hz, 1H), 3.64 (s, 3H), 2.92 (dd, J = 13.4, 6.9 Hz, 2H), 2.24 (t, J = 7.4 Hz, 2H), 1.60–1.40 (m, 4H), 1.34 (s, 12H), 1.32–1.24 (m, 2H).

Methyl 7-((4-(4,4,5,5-tetramethyl-1,3,2-dioxaborolan-2-yl)phenyl)sulfonamido)heptan-oate (4c). *m/z* ($APCI^+$) 426.3 (M + H). ^{1}H NMR (400 MHz, $CDCl_3$) δ 7.92 (d, J = 8.3 Hz, 2H), 7.83 (d, J = 8.3 Hz, 2H), 4.65 (t, J = 6.0 Hz, 1H), 3.64 (s, 3H), 2.91 (dd, J = 13.4, 6.8 Hz, 2H), 2.25 (t, J = 7.4 Hz, 2H), 1.58–1.40 (m, 4H), 1.34 (s, 12H), 1.29–1.22 (m, 4H).

Methyl 8-((4-(4,4,5,5-tetramethyl-1,3,2-dioxaborolan-2-yl)phenyl)sulfonamido)octanoate (4d). ^{1}H NMR (400 MHz, $CDCl_3$) δ 7.92 (d, J = 8.4 Hz, 2H), 7.83 (d, J = 8.4 Hz, 2H), 4.62 (t, J = 6.1 Hz, 1H), 3.64 (s, 3H), 2.91 (dd, J = 13.4, 6.9 Hz, 2H), 2.26 (t, J = 7.5 Hz, 2H), 1.60–1.37 (m, 4H), 1.34 (s, 12H), 1.27–1.15 (m, 6H).

4.3.2. Synthesis and characterization of intermediates 6 and 7

Compound **5** was methylated with methyl iodide to produce the corresponding intermediate **6** according to method VIII, which was then refluxed with hydrazine hydrate (10 equiv.) in methanol for overnight. After that, the solvent was evaporated under reduced pressure and the residue was purified by MPLC to afford the corresponding benzohydrazide derivative **7**.

Methyl 4-(((tert-butoxycarbonyl)(methyl)amino)methyl)benzoate (6). ^{1}H NMR (400 MHz, $CDCl_3$) δ 7.99 (d, J = 8.2 Hz, 2H), 7.27 (d, J = 7.8 Hz, 2H), 4.45 (s, 2H), 3.89 (s, 3H), 2.97–2.65 (m, 3H), 1.60–1.33 (m, 9H).

***Tert*-butyl (4-(hydrazinecarbonyl)benzyl)(methyl)carbamate (7).** ^{1}H NMR (400 MHz, DMSO-d_6) δ 9.70 (s, 1H), 7.78 (d, J = 8.1 Hz, 2H), 7.25 (d, J = 8.2 Hz, 2H), 4.45 (s, 2H), 4.38 (s, 2H), 2.75 (s, 3H), 1.49–1.23 (m, 9H).

4.3.3. Synthesis and characterization of intermediates 10a, b

The pyrazine carboxylic acid **9** was reacted with the appropriate benzohydrazide derivative according to method X to obtain the corresponding 1,3,4-oxadiazole derivatives ***10a, b***.

5-Bromo-3-(5-phenyl-1,3,4-oxadiazol-2-yl)pyrazin-2-amine (10a). ^{1}H NMR (400 MHz, DMSO-d_6) δ 8.40 (s, 1H), 8.07 (dd, J = 8.0, 1.5 Hz, 2H), 7.75 (br, 2H), 7.69–7.56 (m, 3H).

***Tert*-butyl (4-(5-(3-amino-6-bromopyrazin-2-yl)-1,3,4-oxadiazol-2-yl)benzyl)(methyl)-carbamate (10b).** ^{1}H NMR (400 MHz, DMSO-d_6) δ 8.40 (s, 1H), 8.07 (d, J = 8.1 Hz, 2H), 7.76 (br, 2H), 7.45 (d, J = 8.1 Hz, 2H), 4.46 (s, 2H), 2.80 (s, 3H), 1.53–1.23 (m, 9H).

4.3.4. Synthesis and characterization of intermediate 11b

The bromopyrazine derivative **11a** was converted to the corresponding pinacol boronic ester **11b** according to method V.

3-Amino-*N*-phenyl-6-(4,4,5,5-tetramethyl-1,3,2-dioxaborolan-2-yl)pyrazine-2-carboxamide (11b). *m/z* (APCI$^+$) 341.0 (M + H). ^{1}H NMR (400 MHz, DMSO-d_6) δ 10.15 (s, 1H), 8.42 (s, 1H), 7.81 (br, 2H), 7.72 (d, J = 7.7 Hz, 2H), 7.36 (t, J = 7.9 Hz, 2H), 7.12 (t, J = 7.4 Hz, 1H), 1.30 (s, 12H).

4.3.5. Synthesis and characterization of intermediates 12a-e and 13a-d

Pyrazine derivatives **10a, 10b** and **11a** were coupled with the appropriate boronic esters **4a-d** according to method VI, followed by ester hydrolysis according to method II to obtain the corresponding acids **12a-e** and **13a-d**.

5-((4-(5-Amino-6-(5-phenyl-1,3,4-oxadiazol-2-yl)pyrazin-2-yl) phenyl)sulfonamido) pentanoic acid (12a). ^{1}H NMR (400 MHz, DMSO-d_6) δ 11.96 (s, 1H), 8.99 (s, 1H), 8.29 (d, J = 8.5 Hz, 2H), 8.15 (dd, J = 7.6, 1.6 Hz, 2H), 7.88 (d, J = 8.5 Hz, 2H), 7.83 (br, 2H), 7.72–7.57 (m, 4H), 2.76 (dd, J = 12.6, 6.4 Hz, 2H), 2.14 (t, J = 7.0 Hz, 2H), 1.55–1.31 (m, 4H).

6-((4-(5-Amino-6-(5-phenyl-1,3,4-oxadiazol-2-yl)pyrazin-2-yl) phenyl)sulfonamido) hexanoic acid (12b). ^{1}H NMR (400 MHz, DMSO-d_6) δ 11.95 (s, 1H), 8.99 (s, 1H), 8.29 (d, J = 8.6 Hz, 2H), 8.16 (dd, J = 7.8, 1.7 Hz, 2H), 7.89 (d, J = 8.6 Hz, 2H), 7.82 (br, 2H), 7.71–7.57 (m, 4H), 2.75 (dd, J = 13.0, 6.8 Hz, 2H), 2.12 (t, J = 7.3 Hz, 2H), 1.47–1.31 (m, 4H), 1.28–1.13 (m, 2H).

5-((4-(5-Amino-6-(5-(4-(((tert-butoxycarbonyl)(methyl)amino) methyl)phenyl)-1,3,4-oxadiazol-2-yl)pyrazin-2-yl)phenyl)sulfonamido)pentanoic acid (12c). ^{1}H NMR (400 MHz, DMSO-d_6) δ 11.96 (s, 1H), 8.99 (s, 1H), 8.30 (d, J = 8.6 Hz, 2H), 8.14 (d, J = 8.1 Hz, 2H), 7.88 (d, J = 8.6 Hz, 2H), 7.82 (br, 2H), 7.64 (t, J = 5.9 Hz, 1H), 7.47 (d, J = 8.2 Hz, 2H), 4.48 (s, 2H), 2.81 (s, 3H), 2.76 (dd, J = 12.8, 6.6 Hz, 2H), 2.14 (t, J = 7.1 Hz, 2H), 1.56–1.26 (m, 13H).

6-((4-(5-Amino-6-(5-(4-(((tert-butoxycarbonyl)(methyl)amino) methyl)phenyl)-1,3,4-oxadiazol-2-yl)pyrazin-2-yl)phenyl)sulfonamido)hexanoic acid (12d). ^{1}H NMR (400 MHz, DMSO-d_6) δ 11.93 (s, 1H), 8.99 (s, 1H), 8.30 (d, J = 8.6 Hz, 2H), 8.14 (d, J = 8.1 Hz, 2H), 7.88 (d, J = 8.6 Hz, 2H), 7.83 (br, 2H), 7.62 (t, J = 5.1 Hz, 1H), 7.47 (d, J = 8.2 Hz, 2H), 4.48 (s, 2H), 2.81 (s, 3H), 2.75 (dd, J = 13.0, 6.8 Hz, 2H), 2.12 (t, J = 7.3 Hz, 2H), 1.49–1.31 (m, 13H), 1.27–1.16 (m, 2H).

7-((4-(5-Amino-6-(5-(4-(((tert-butoxycarbonyl)(methyl)amino) methyl)phenyl)-1,3,4-oxadiazol-2-yl)pyrazin-2-yl)phenyl)sulfonamido)heptanoic acid (12e). ^{1}H NMR (400 MHz, DMSO-d_6) δ 11.90 (s, 1H), 8.99 (s, 1H), 8.30 (d, J = 8.5 Hz, 2H), 8.15 (d, J = 8.1 Hz, 2H), 7.88 (d, J = 8.6 Hz, 2H), 7.83 (br, 2H), 7.61 (t, J = 5.8 Hz, 1H), 7.48 (d, J = 8.2 Hz, 2H), 4.48 (s, 2H), 2.81 (s, 3H), 2.75 (dd, J = 13.0, 6.8 Hz, 2H), 2.13 (t, J = 7.4 Hz, 2H), 1.52–1.30 (m, 13H), 1.27–1.12 (m, 4H).

5-((4-(5-Amino-6-(phenylcarbamoyl)pyrazin-2-yl)phenyl)sulfonamido)pentanoic acid (13a). ^{1}H NMR (400 MHz, DMSO-d_6) δ 11.96 (s, 1H), 10.41 (s, 1H), 8.98 (s, 1H), 8.42 (d, J = 8.5 Hz, 2H), 7.93–7.72 (m, 6H), 7.63 (t, J = 5.8 Hz, 1H), 7.39 (t, J = 7.9 Hz, 2H), 7.15 (t, J = 7.4 Hz, 1H), 2.74 (dd, J = 12.8, 6.5 Hz, 2H), 2.14 (t, J = 7.1 Hz, 2H), 1.52–1.31 (m, 4H).

6-((4-(5-Amino-6-(phenylcarbamoyl)pyrazin-2-yl)phenyl)sulfonamido)hexanoic acid (13b). ^{1}H NMR (400 MHz, DMSO-d_6) δ 11.93 (s, 1H), 10.40 (s, 1H), 8.98 (s, 1H), 8.42 (d, J = 8.4 Hz, 2H), 7.91–7.71 (m, 6H), 7.61 (t, J = 5.8 Hz, 1H), 7.38 (t, J = 7.8 Hz, 2H), 7.15 (t, J = 7.4 Hz, 1H), 2.73 (dd, J = 13.0, 6.6 Hz, 2H), 2.12 (t, J = 7.3 Hz, 2H), 1.46–1.31 (m, 4H), 1.27–1.15 (m, 2H).

7-((4-(5-Amino-6-(phenylcarbamoyl)pyrazin-2-yl)phenyl)sulfonamido)heptanoic acid (13c). ^{1}H NMR (400 MHz, DMSO-d_6) δ 11.95 (s, 1H), 10.40 (s, 1H), 8.98 (s, 1H), 8.42 (d, J = 8.5 Hz, 2H), 7.92–7.71 (m, 6H), 7.61 (t, J = 5.8 Hz, 1H), 7.38 (t, J = 7.9 Hz, 2H), 7.14 (t, J = 7.4 Hz, 1H), 2.73 (dd, J = 13.0, 6.8 Hz, 2H), 2.13 (t, J = 7.4 Hz, 2H), 1.47–1.30 (m, 4H), 1.25–1.12 (m, 4H).

8-((4-(5-Amino-6-(phenylcarbamoyl)pyrazin-2-yl)phenyl)sulfonamido)octanoic acid (13d). ^{1}H NMR (400 MHz, DMSO-d_6) δ 11.92 (s, 1H), 10.40 (s, 1H), 8.98 (s, 1H), 8.42 (d, J = 8.5 Hz, 2H), 7.95–7.73 (m, 6H), 7.60 (t, J = 5.8 Hz, 1H), 7.39 (t, J = 7.9 Hz, 2H), 7.15 (t, J = 7.4 Hz, 1H), 2.73 (dd, J = 13.0, 6.7 Hz, 2H), 2.13 (t, J = 7.4 Hz, 2H), 1.46–1.30 (m, 4H), 1.24–1.11 (m, 6H).

4.3.6. Synthesis and characterization of intermediates 13e and 13f

Pyrazine boronic ester derivative **11b** was coupled with the appropriate 4-bromobenzene sulfonamide derivatives **3e** and **3f** according to method VI, followed by ester hydrolysis according to method III to obtain the corresponding acids **13e** and **13f**.

3-(2-(2-((4-(5-Amino-6-(phenylcarbamoyl)pyrazin-2-yl)phenyl) sulfonamido)ethoxy) ethoxy)propanoic acid (13e). ^{1}H NMR (400 MHz, DMSO-d_6) δ 12.11 (br, 1H), 10.40 (s, 1H), 8.98 (s, 1H), 8.41 (d, J = 8.3 Hz, 2H), 7.95–7.68 (m, 7H), 7.38 (t, J = 7.7 Hz, 2H), 7.15 (t, J = 7.2 Hz, 1H), 3.55 (t, J = 6.2 Hz, 2H), 3.48–3.37 (m, 6H), 2.91 (dd, J = 11.3, 5.5 Hz, 2H), 2.39 (t, J = 6.2 Hz, 2H).

3-(2-(2-(2-((4-(5-Amino-6-(phenylcarbamoyl)pyrazin-2-yl) phenyl)sulfonamido)ethoxy) ethoxy)ethoxy)propanoic acid (13f). ^{1}H NMR (400 MHz, DMSO-d_6) δ 12.10 (br, 1H), 10.39 (s, 1H), 8.97 (s, 1H), 8.40 (d, J = 8.0 Hz, 2H), 7.91–7.69 (m, 7H), 7.37 (t, J = 7.5 Hz, 2H), 7.13 (t, J = 7.1 Hz, 1H), 3.54 (t, J = 6.0 Hz, 2H), 3.48–3.34 (m, 10H), 2.90 (dd, J = 11.3, 5.8 Hz, 2H), 2.38 (t, J = 6.0 Hz, 2H).

4.3.7. Synthesis and characterization of intermediates 29-31

Intermediate **28** was reacted with *N*-Boc-2-bromoethylamine to produce the corresponding alkylated derivative **29** according to method VIII, followed by a hydrogenation reaction according to method IX to produce the intermediate compound **30**. Finally, Boc-deprotection according to method VII-A afforded the phenyl-glutarimide derivative **31.**

***Tert*-butyl (2-(4-(2,6-bis(benzyloxy)pyridin-3-yl)phenoxy)ethyl)carbamate (29).** ^{1}H NMR (400 MHz, DMSO-d_6) δ 7.69 (d, J = 8.1 Hz, 1H), 7.52–7.25 (m, 12H), 7.03–6.91 (m, 3H), 6.53 (d, J = 8.1 Hz, 1H), 5.40 (s, 2H), 5.36 (s, 2H), 3.98 (t, J = 5.8 Hz, 2H), 3.31–3.26 (m, 2H), 1.39 (s, 9H).

***Tert*-butyl (2-(4-(2,6-dioxopiperidin-3-yl)phenoxy)ethyl)carbamate (30).** ^{1}H NMR (400 MHz, DMSO-d_6) δ 10.78 (s, 1H), 7.13 (d, J = 8.6 Hz, 2H), 7.01–6.95 (m, 1H), 6.89 (d, J = 8.6 Hz, 2H), 3.95 (t, J = 5.8 Hz, 2H), 3.79 (dd, J = 11.3, 4.9 Hz, 1H), 3.29 (dd, J = 11.8, 6.0 Hz, 2H), 2.69–2.59 (m, 1H), 2.50–2.41 (m, 1H), 2.21–2.10 (m, 1H), 2.06–1.96 (m, 1H), 1.39 (s, 9H).

3-(4-(2-Aminoethoxy)phenyl)piperidine-2,6-dione (31). ^{1}H NMR (400 MHz, DMSO-d_6) δ 10.77 (s, 1H), 8.37–8.13 (m, 3H), 7.14 (d, J = 8.7 Hz, 2H), 6.93 (d, J = 8.7 Hz, 2H), 4.16 (t, J = 5.2 Hz, 2H), 3.79 (dd, J = 11.4, 4.9 Hz, 1H), 3.24–3.09 (m, 2H), 2.68–2.58 (m, 1H),

2.48–2.41 (m, 1H), 2.21–2.07 (m, 1H), 2.04–1.94 (m, 1H).

4.3.8. Synthesis and characterization of intermediates 33–35

The 6-fluoropicolinic acid **32** was refluxed in 5 mL of thionyl chloride for 2 h. Then the solvent was evaporated under reduced pressure to produce the corresponding acid chloride which was reacted with 3-aminopiperidine-2,6-dione according to method I to afford the intermediate compound **33**. The later was then converted to its piperazine analogue **34** through its reaction with 1-Boc-piperazine according to method XI. Finally, Boc-deprotection according to method VII-A afforded the picolinamide glutarimide derivative **35.**

***N*-(2,6-dioxopiperidin-3-yl)-6-fluoropicolinamide *(33)*.** ^{1}H NMR (400 MHz, DMSO-d_6) δ 10.84 (s, 1H), 8.97 (d, J = 8.5 Hz, 1H), 8.19 (dd, J = 15.6, 8.1 Hz, 1H), 8.03–7.95 (m, 1H), 7.44 (dd, J = 8.2, 1.8 Hz, 1H), 4.82–4.71 (m, 1H), 2.84–2.73 (m, 1H), 2.57–2.49 (m, 1H), 2.31–2.13 (m, 1H), 2.01–1.90 (m, 1H).

***Tert-butyl 4-(6-((2,6-dioxopiperidin*-3-yl*)carbamoyl)pyridin*-2-yl*)piperazine-1-carboxylate (34)*.** ^{1}H NMR (400 MHz, DMSO-d_6) δ 10.86 (s, 1H), 8.76 (d, J = 8.5 Hz, 1H), 7.70 (dd, J = 8.5, 7.3 Hz, 1H), 7.32 (d, J = 7.1 Hz, 1H), 7.03 (d, J = 8.5 Hz, 1H), 4.79–4.67 (m, 1H), 3.64–3.51 (m, 4H), 3.49–3.37 (m, 4H), 2.86–2.72 (m, 1H), 2.57–2.50 (m, 1H), 2.30–2.16 (m, 1H), 2.01–1.92 (m, 1H), 1.41 (s, 9H).

***N-(2,6-dioxopiperidin*-3-yl*)-6-(piperazin*-1-yl*)picolinamide (35)*.** ^{1}H NMR (400 MHz, DMSO-d_6) δ 10.86 (s, 1H), 9.48 (s, 2H), 8.80 (d, J = 8.5 Hz, 1H), 7.75 (dd, J = 8.5, 7.4 Hz, 1H), 7.38 (d, J = 7.2 Hz, 1H), 7.12 (d, J = 8.5 Hz, 1H), 4.81–4.65 (m, 1H), 3.92–3.78 (m, 4H), 3.16 (s, 4H), 2.86–2.71 (m, 1H), 2.59–2.49 (m, 1H), 2.32–2.14 (m, 1H), 2.02–1.91 (m, 1H).

4.3.9. Synthesis and characterization of the reference inhibitor 13g

Pyrazine boronic ester derivative **11b** was coupled with 4-bromobenzene sulfonamide derivatives **3g** according to method VI to obtain the control inhibitor **13g**.

3-Amino-6-(4-(N-methylsulfamoyl)phenyl)-N-phenylpyrazine-2-carboxamide 13g. ^{1}H NMR (400 MHz, DMSO-d_6) δ 10.41 (s, 1H), 8.99 (s, 1H), 8.43 (d, J = 8.5 Hz, 2H), 7.91–7.75 (m, 6H), 7.49 (q, J = 4.9 Hz, 1H), 7.38 (t, J = 7.9 Hz, 2H), 7.15 (t, J = 7.4 Hz, 1H), 2.43 (d, J = 5.0 Hz, 3H). ^{13}C NMR (101 MHz, DMSO-d_6) δ 164.81, 155.10, 145.66, 139.94, 138.81, 138.27, 137.17, 129.05, 127.52, 126.62, 124.79, 124.72, 121.67, 29.11. HRMS (ESI, positive): Calcd. for $C_{18}H_{18}N_5O_3S$ $[M+H]^+$: m/z = 384.112; Found: 384.112. HPLC t_R = 12.79 min (purity 96 %).

4.3.10. Synthesis and characterization of the final PROTACs

The linker-connected ATR inhibitors (**12a-e** and **13a-f)** were reacted with the appropriate E3 ligase ligand (**20a-c, 25, 31, 35** and **41),** according to method IV. In case of coupling with **12c-d, t**he amide coupling reaction was followed by the removal of Boc-protecting group according to method VII-B.

Analyses indicated by the symbols of the elements or functions were within ±0.4 % of the theoretical values.

6-((4-(5-Amino-6-(5-phenyl-1,3,4-oxadiazol-2-yl)pyrazin-2-yl) phenyl)sulfonamido)-N-(3-(2-(2,6-dioxopiperidin-3-yl)-1-oxoisoindolin-4-yl)prop-2-yn-1-yl)hexanamide 42a. ^{1}H NMR (400 MHz, DMSO-d_6) δ 10.97 (s, 1H), 8.99 (s, 1H), 8.29 (d, J = 8.5 Hz, 3H), 8.16 (dd, J = 7.6, 1.8 Hz, 2H), 7.88 (d, J = 8.5 Hz, 2H), 7.84 (br, 2H), 7.74–7.56 (m, 6H), 7.50 (t, J = 7.6 Hz, 1H), 5.12 (dd, J = 13.3, 5.1 Hz, 1H), 4.41 (d, J = 17.7 Hz, 1H), 4.28 (d, J = 17.7 Hz, 1H), 4.12 (d, J = 5.3 Hz, 2H), 2.96–2.82 (m, 1H), 2.74 (dd, J = 13.0, 6.7 Hz, 2H), 2.63–2.50 (m, 1H), 2.45–2.31 (m, 1H), 2.06 (t, J = 7.4 Hz, 2H), 2.03–1.93 (m, 1H), 1.47–1.31 (m, 4H), 1.29–1.19 (m, 2H). ^{13}C NMR (101 MHz, DMSO-d_6) δ 173.24, 172.30, 171.38, 167.95, 164.43, 163.29, 153.25, 144.37, 144.22, 140.30, 139.89, 138.60, 134.57, 132.87, 132.44, 130.00, 129.10, 127.57, 127.41, 126.22, 123.62, 123.48, 120.21, 118.31, 93.02, 77.77, 52.05, 47.32, 42.91, 35.42, 31.62, 29.26, 29.06, 26.19, 25.11, 22.88. HRMS (ESI, positive): Calcd. for $C_{40}H_{38}N_9O_7S$ $[M+H]^+$: m/z = 788.261; Found: 788.262. HPLC t_R = 13.49 min (purity 95.0 %).

5-((4-(5-Amino-6-(5-phenyl-1,3,4-oxadiazol-2-yl)pyrazin-2-yl) phenyl)sulfonamido)-N-(3-(2-(2,6-dioxopiperidin-3-yl)-1-oxoisoindolin-4-yl)prop-2-yn-1-yl)pentanamide 42b. ^{1}H NMR (400 MHz, DMSO-d_6) δ 10.99 (s, 1H), 8.99 (s, 1H), 8.31 (dd, J = 12.5, 6.9 Hz, 3H), 8.15 (dd, J = 7.7, 1.7 Hz, 2H), 7.88 (d, J = 8.5 Hz, 2H), 7.84 (br, 2H), 7.73–7.58 (m, 6H), 7.50 (t, J = 7.6 Hz, 1H), 5.12 (dd, J = 13.3, 5.1 Hz, 1H), 4.41 (d, J = 17.8 Hz, 1H), 4.28 (d, J = 17.8 Hz, 1H), 4.12 (d, J = 5.3 Hz, 2H), 2.95–2.84 (m, 1H), 2.76 (dd, J = 13.0, 6.7 Hz, 2H), 2.62–2.51 (m, 1H), 2.46–2.34 (m, 1H), 2.07 (t, J = 7.2 Hz, 2H), 2.02–1.95 (m, 1H), 1.53–1.43 (m, 2H), 1.43–1.32 (m, 2H). ^{13}C NMR (101 MHz, DMSO-d_6) δ 173.28, 172.17, 171.41, 167.96, 164.41, 163.26, 153.23, 144.35, 144.21, 140.30, 139.88, 138.57, 134.60, 132.87, 132.43, 129.99, 129.10, 127.57, 127.39, 126.21, 123.63, 123.46, 120.18, 118.28, 92.93, 77.80, 52.05, 47.33, 42.79, 34.95, 31.61, 29.12, 29.07, 22.87, 22.74. HRMS (ESI, positive): Calcd. for $C_{39}H_{36}N_9O_7S$ $[M+H]^+$: m/z = 774.245; Found: 774.245. HPLC t_R = 13.31 min (purity 100 %).

1-(4-(5-(3-Amino-6-(4-(N-(5-((5-(2-(2,6-dioxopiperidin-3-yl)-1-oxoisoindolin-4-yl)pent-4-yn-1-yl)amino)-5-oxopentyl)sulfamoyl) phenyl)pyrazin-2-yl)-1,3,4-oxadiazol-2-yl)phenyl)-N-methylmethanaminium formate 42c

^{1}H NMR (400 MHz, DMSO-d_6) δ 10.93 (br, 1H), 8.99 (s, 1H), 8.30 (d, J = 8.6 Hz, 2H), 8.24 (s, 1H), 8.12 (d, J = 8.3 Hz, 2H), 7.93–7.74 (m, 5H), 7.64 (dd, J = 11.1, 4.6 Hz, 4H), 7.56 (dd, J = 7.6, 1.0 Hz, 1H), 7.46 (t, J = 7.6 Hz, 1H), 5.11 (dd, J = 13.2, 5.1 Hz, 1H), 4.42 (d, J = 17.9 Hz, 1H), 4.28 (d, J = 17.9 Hz, 1H), 3.89 (s, 2H), 3.14 (dd, J = 13.0, 6.6 Hz, 2H), 2.94–2.83 (m, 1H), 2.75 (t, J = 6.5 Hz, 2H), 2.59–2.52 (m, 1H), 2.43 (dd, J = 12.7, 5.7 Hz, 3H), 2.37 (s, 3H), 2.02–1.93 (m, 3H), 1.67–1.57 (m, 2H), 1.49–1.39 (m, 2H), 1.39–1.29 (m, 2H). ^{13}C NMR (101 MHz, DMSO-d_6) δ 173.26, 172.21, 171.37, 168.07, 164.57, 164.35, 163.20, 153.24, 144.32, 144.18, 143.32, 140.38, 139.87, 138.57, 134.28, 132.35, 129.93, 128.93, 127.56, 127.38, 126.20, 123.02, 122.34, 120.19, 119.12, 96.15, 77.01, 53.82, 52.03, 47.41, 42.81, 37.95, 35.23, 34.89, 31.65, 29.17, 28.63, 22.82, 22.74, 16.86. HRMS (ESI, positive): Calcd. for $C_{43}H_{45}N_{10}O_7S$ $[M+H]^+$: m/z = 845.319; Found: 845.319. HPLC t_R = 11.16 min (purity 95.3 %).

1-(4-(5-(3-Amino-6-(4-(N-(6-((5-(2-(2,6-dioxopiperidin-3-yl)-1-oxoisoindolin-4-yl)pent-4-yn-1-yl)amino)-6-oxohexyl)sulfamoyl) phenyl)pyrazin-2-yl)-1,3,4-oxadiazol-2-yl)phenyl)-N-methylmethanaminium formate 42d. ^{1}H NMR (400 MHz, DMSO-d_6) δ 10.93 (br, 1H), 8.99 (s, 1H), 8.29 (d, J = 8.6 Hz, 2H), 8.22 (s, 1H), 8.16 (d, J = 8.3 Hz, 2H), 7.93–7.74 (m, 5H), 7.70–7.55 (m, 5H), 7.47 (t, J = 7.6 Hz, 1H), 5.11 (dd, J = 13.1, 5.1 Hz, 1H), 4.43 (d, J = 17.9 Hz, 1H), 4.28 (d, J = 17.9 Hz, 1H), 4.05 (s, 2H), 3.15 (dd, J = 12.8, 6.6 Hz, 2H), 2.94–2.84 (m, 1H), 2.74 (t, J = 6.3 Hz, 2H), 2.60–2.51 (m, 1H), 2.47–2.37 (m, 6H), 1.99 (t, J = 7.3 Hz, 3H), 1.68–1.59 (m, 2H), 1.44–1.32 (m, 4H), 1.24–1.14 (m, 2H). ^{13}C NMR (101 MHz, DMSO-d_6) δ 173.25, 172.40, 171.38, 168.08, 164.49, 164.21, 163.30, 153.26, 144.32, 144.25, 140.48, 140.32, 139.87, 138.60, 134.31, 132.36, 130.51, 128.95, 127.57, 127.52, 126.22, 123.01, 120.14, 119.15, 96.18, 77.00, 52.72, 52.04, 47.42, 42.94, 37.93, 35.70, 33.95, 31.66, 29.23, 28.59, 26.21, 25.22, 22.75, 16.85. HRMS (ESI, positive): Calcd. for $C_{44}H_{47}N_{10}O_7S$ $[M+H]^+$: m/z = 859.334; Found: 859.334. HPLC t_R = 12.12 min (purity 95.4 %).

1-(4-(5-(3-Amino-6-(4-(N-(7-((5-(2-(2,6-dioxopiperidin-3-yl)-1-oxoisoindolin-4-yl)pent-4-yn-1-yl)amino)-7-oxoheptyl)sulfamoyl) phenyl)pyrazin-2-yl)-1,3,4-oxadiazol-2-yl)phenyl)-N-methylmethanaminium formate 42e. ^{1}H NMR (400 MHz, DMSO-d_6) δ 10.94 (br, 1H), 8.99 (s, 1H), 8.31–8.25 (m, 3H), 8.12 (d, J = 8.2 Hz, 2H), 7.96–7.72 (m, 5H), 7.70–7.54 (m, 5H), 7.47 (t, J = 7.6 Hz, 1H), 5.11 (dd, J = 13.1, 5.1 Hz, 1H), 4.43 (d, J = 17.9 Hz, 1H), 4.28 (d, J = 17.8 Hz, 1H), 3.89 (s, 2H), 3.15 (dd, J = 12.8, 6.7 Hz, 2H), 2.95–2.84 (m, 1H), 2.74 (t, J = 6.6 Hz, 2H), 2.60–2.52 (m, 1H), 2.43 (t, J = 7.0 Hz, 3H), 2.37 (s, 3H), 1.99 (t, J = 7.4 Hz, 3H), 1.69–1.58 (m, 2H), 1.45–1.30 (m, 4H), 1.24–1.08 (m, 4H). ^{13}C NMR (101 MHz, DMSO-d_6) δ 173.24, 172.47, 171.38, 168.09, 164.81, 164.36, 163.21, 153.24, 144.32, 144.18,

143.41, 140.35, 139.88, 138.59, 134.32, 132.37, 129.91, 128.95, 127.57, 127.38, 126.21, 123.04, 122.32, 120.20, 119.16, 96.17, 77.00, 53.84, 52.03, 47.42, 42.98, 37.92, 35.73, 34.91, 31.66, 29.35, 28.60, 26.22, 25.54, 22.75, 16.85. HRMS (ESI, positive): Calcd. for $C_{45}H_{49}N_{10}O_7S$ $[M+H]^+$: m/z = 873.350; Found: 873.350. HPLC t_R = 12.41 min (purity 95.9 %).

1-(4-(5-(3-Amino-6-(4-(N-(7-((3-(2-(2,6-dioxopiperidin-3-yl)-1-oxoisoindolin-4-yl)prop-2-yn-1-yl)amino)-7-oxoheptyl)sulfamoyl)phenyl)pyrazin-2-yl)-1,3,4-oxadiazol-2-yl)phenyl)-N-methylmethanaminium formate 42f. ^{1}H NMR (400 MHz, DMSO-d_6) δ 10.91 (br, 1H), 8.92 (s, 1H), 8.22 (d, J = 8.5 Hz, 3H), 8.17 (s, 1H), 8.06 (d, J = 8.2 Hz, 2H), 7.81 (d, J = 8.4 Hz, 2H), 7.76 (br, 2H), 7.64 (d, J = 7.6 Hz, 1H), 7.60–7.49 (m, 4H), 7.43 (t, J = 7.6 Hz, 1H), 5.05 (dd, J = 13.3, 5.0 Hz, 1H), 4.34 (d, J = 17.7 Hz, 1H), 4.20 (d, J = 17.8 Hz, 1H), 4.04 (d, J = 5.3 Hz, 2H), 3.82 (s, 2H), 2.88–2.76 (m, 1H), 2.72–2.63 (m, 2H), 2.56–2.45 (m, 1H), 2.38–2.22 (m, 4H), 1.99 (t, J = 7.4 Hz, 2H), 1.96–1.88 (m, 1H), 1.41–1.32 (m, 2H), 1.32–1.23 (m, 2H), 1.19–1.04 (m, 4H). ^{13}C NMR (101 MHz, DMSO-d_6) δ 173.15, 172.29, 171.29, 167.86, 164.47, 164.28, 163.12, 153.15, 144.26, 144.10, 143.40, 140.27, 139.79, 138.50, 134.46, 132.34, 129.80, 129.01, 127.48, 127.30, 126.13, 123.52, 122.22, 120.12, 118.22, 92.95, 77.65, 53.81, 51.95, 47.21, 42.87, 35.34, 34.88, 31.52, 29.21, 28.95, 28.47, 26.12, 25.33, 22.80. HRMS (ESI, positive): Calcd. for $C_{43}H_{45}N_{10}O_7S$ $[M+H]^+$: m/z = 845.319; Found: 845.318. HPLC t_R = 11.99 min (purity 94.2 %).

1-(4-(5-(3-Amino-6-(4-(N-(6-((3-(2-(2,6-dioxopiperidin-3-yl)-1-oxoisoindolin-4-yl)prop-2-yn-1-yl)amino)-6-oxohexyl)sulfamoyl)phenyl)pyrazin-2-yl)-1,3,4-oxadiazol-2-yl)phenyl)-N-methylmethanaminium formate 42g. ^{1}H NMR (400 MHz, DMSO-d_6) δ 10.94 (br, 1H), 8.99 (s, 1H), 8.30 (m, 3H), 8.22 (s, 1H), 8.14 (d, J = 8.2 Hz, 2H), 7.88 (d, J = 8.5 Hz, 2H), 7.84 (br, 2H), 7.71 (d, J = 7.5 Hz, 1H), 7.63 (dd, J = 13.0, 7.9 Hz, 4H), 7.50 (t, J = 7.6 Hz, 1H), 5.12 (dd, J = 13.3, 5.1 Hz, 1H), 4.41 (d, J = 17.7 Hz, 1H), 4.28 (d, J = 17.7 Hz, 1H), 4.12 (d, J = 5.3 Hz, 2H), 3.93 (s, 2H), 2.96–2.83 (m, 1H), 2.74 (t, J = 6.0 Hz, 2H), 2.62–2.51 (m, 1H), 2.45–2.29 (m, 4H), 2.06 (t, J = 7.4 Hz, 2H), 2.02–1.94 (m, 1H), 1.48–1.32 (m, 4H), 1.27–1.16 (m, 2H). ^{13}C NMR (101 MHz, DMSO-d_6) δ 173.24, 172.30, 171.39, 167.95, 164.47, 164.34, 163.24, 153.26, 144.37, 144.22, 140.30, 139.89, 138.60, 134.57, 132.44, 130.05, 129.10, 127.58, 127.43, 126.23, 123.62, 122.49, 120.20, 118.31, 93.03, 77.77, 53.63, 52.05, 47.32, 42.91, 35.42, 34.74, 31.62, 29.25, 29.06, 26.19, 25.12, 22.88. HRMS (ESI, positive): Calcd. for $C_{42}H_{43}N_{10}O_7S$ $[M+H]^+$: m/z = 831.303; Found: 831.303. HPLC t_R = 11.68 min (purity 95.1 %).

3-Amino-6-(4-(N-(6-((3-(2-(2,6-dioxopiperidin-3-yl)-1-oxoisoindolin-4-yl)prop-2-yn-1-yl)amino)-6-oxohexyl)sulfamoyl)phenyl)-N-phenylpyrazine-2-carboxamide 42h. ^{1}H NMR (400 MHz, DMSO-d_6) δ 10.98 (s, 1H), 10.40 (s, 1H), 8.98 (s, 1H), 8.41 (d, J = 8.5 Hz, 2H), 8.30 (t, J = 5.3 Hz, 1H), 7.91–7.75 (m, 6H), 7.72 (d, J = 7.1 Hz, 1H), 7.65–7.57 (m, 2H), 7.51 (t, J = 7.6 Hz, 1H), 7.38 (t, J = 7.9 Hz, 2H), 7.15 (t, J = 7.4 Hz, 1H), 5.13 (dd, J = 13.3, 5.1 Hz, 1H), 4.42 (d, J = 17.8 Hz, 1H), 4.29 (d, J = 17.7 Hz, 1H), 4.12 (d, J = 5.3 Hz, 2H), 2.95–2.83 (m, 1H), 2.72 (dd, J = 13.0, 6.7 Hz, 2H), 2.64–2.52 (m, 1H), 2.46–2.33 (m, 1H), 2.06 (t, J = 7.4 Hz, 2H), 2.02–1.94 (m, 1H), 1.48–1.32 (m, 4H), 1.28–1.17 (m, 2H). ^{13}C NMR (101 MHz, DMSO-d_6) δ 173.24, 172.29, 171.39, 167.96, 164.82, 155.09, 145.65, 144.38, 140.08, 139.78, 138.27, 137.17, 134.59, 132.46, 129.11, 129.05, 127.31, 126.57, 124.77, 124.72, 123.63, 121.68, 118.32, 93.03, 77.79, 52.06, 47.33, 42.91, 35.42, 31.62, 29.25, 29.06, 26.20, 25.11, 22.89. HRMS (ESI, positive): Calcd. for $C_{39}H_{39}N_8O_7S$ $[M+H]^+$: m/z = 763.266; Found: 763.266. HPLC t_R = 13.11 min (purity 96.6 %).

3-Amino-6-(4-(N-(6-((5-(2-(2,6-dioxopiperidin-3-yl)-1-oxoisoindolin-4-yl)pent-4-yn-1-yl)amino)-6-oxohexyl)sulfamoyl)phenyl)-N-phenylpyrazine-2-carboxamide 42i. ^{1}H NMR (400 MHz, DMSO-d_6) δ 10.95 (s, 1H), 10.40 (s, 1H), 8.97 (s, 1H), 8.41 (d, J = 8.5 Hz, 2H), 7.88–7.74 (m, 7H), 7.68 (d, J = 7.4 Hz, 1H), 7.63–7.56 (m, 2H), 7.48 (t, J = 7.6 Hz, 1H), 7.38 (t, J = 7.9 Hz, 2H), 7.14 (t, J = 7.4 Hz, 1H), 5.12 (dd, J = 13.1, 5.0 Hz, 1H), 4.44 (d, J = 17.9 Hz, 1H), 4.29 (d, J = 17.9 Hz, 1H), 3.16 (dd, J = 12.7, 6.6 Hz, 2H), 2.95–2.84 (m, 1H), 2.72 (dd, J = 13.0, 6.7 Hz, 2H), 2.61–2.50 (m, 1H), 2.45 (t, J = 7.2 Hz, 3H), 1.99 (t, J = 7.3 Hz, 3H), 1.72–1.60 (m, 2H), 1.44–1.29 (m, 4H), 1.24–1.14 (m, 2H). ^{13}C NMR (101 MHz, DMSO-d_6) δ 173.26, 172.40, 171.39, 168.10, 164.81, 155.08, 145.63, 144.33, 140.10, 139.78, 138.26, 137.17, 134.35, 132.38, 129.05, 128.97, 127.32, 126.56, 124.76, 123.05, 121.66, 119.18, 96.20, 77.02, 52.04, 47.43, 42.94, 37.95, 35.71, 31.65, 29.24, 28.61, 26.23, 25.23, 22.76, 16.86. HRMS (ESI, positive): Calcd. for $C_{41}H_{43}N_8O_7S$ $[M+H]^+$: m/z = 791.297; Found: 791.296. HPLC t_R = 13.51 min (purity 97.4 %).

3-Amino-6-(4-(N-(7-((5-(2-(2,6-dioxopiperidin-3-yl)-1-oxoisoindolin-4-yl)pent-4-yn-1-yl)amino)-7-oxoheptyl)sulfamoyl)phenyl)-N-phenylpyrazine-2-carboxamide 42j. ^{1}H NMR (400 MHz, DMSO-d_6) δ 10.95 (s, 1H), 10.40 (s, 1H), 8.98 (s, 1H), 8.41 (d, J = 8.6 Hz, 2H), 7.89–7.72 (m, 7H), 7.68 (dd, J = 7.5, 0.7 Hz, 1H), 7.60 (t, J = 6.1 Hz, 2H), 7.48 (t, J = 7.6 Hz, 1H), 7.41–7.34 (m, 2H), 7.14 (t, J = 7.4 Hz, 1H), 5.12 (dd, J = 13.1, 5.1 Hz, 1H), 4.44 (d, J = 17.9 Hz, 1H), 4.29 (d, J = 17.8 Hz, 1H), 3.16 (dd, J = 12.8, 6.7 Hz, 2H), 2.96–2.84 (m, 1H), 2.73 (dd, J = 13.1, 6.7 Hz, 2H), 2.61–2.51 (m, 1H), 2.44 (t, J = 6.9 Hz, 3H), 2.03–1.93 (m, 3H), 1.71–1.59 (m, 2H), 1.43–1.30 (m, 4H), 1.24–1.10 (m, 4H). ^{13}C NMR (101 MHz, DMSO-d_6) δ 173.25, 172.48, 171.39, 168.10, 164.80, 155.08, 145.62, 144.33, 140.14, 139.77, 138.26, 137.17, 134.34, 132.38, 129.04, 128.96, 127.31, 126.55, 124.76, 124.71, 123.05, 121.66, 119.18, 96.19, 77.02, 52.04, 47.43, 42.98, 37.93, 35.74, 31.66, 29.34, 28.61, 26.24, 25.55, 22.76, 16.86. HRMS (ESI, positive): Calcd. for $C_{42}H_{45}N_8O_7S$ $[M+H]^+$: m/z = 805.313; Found: 805.314. HPLC t_R = 13.83 min (purity 97.2 %).

3-Amino-6-(4-(N-(5-((5-(2-(2,6-dioxopiperidin-3-yl)-1-oxoisoindolin-4-yl)pent-4-yn-1-yl)amino)-5-oxopentyl)sulfamoyl)phenyl)-N-phenylpyrazine-2-carboxamide 42k. ^{1}H NMR (500 MHz, DMSO-d_6) δ 11.00 (s, 1H), 10.44 (s, 1H), 9.03 (s, 1H), 8.46 (d, J = 8.5 Hz, 2H), 7.92–7.79 (m, 7H), 7.72 (d, J = 7.6 Hz, 1H), 7.70–7.61 (m, 2H), 7.53 (t, J = 7.6 Hz, 1H), 7.43 (t, J = 7.9 Hz, 2H), 7.22–7.17 (m, 1H), 5.17 (dd, J = 13.3, 4.9 Hz, 1H), 4.48 (d, J = 17.8 Hz, 1H), 4.34 (d, J = 17.8 Hz, 1H), 3.20 (dd, J = 12.6, 6.3 Hz, 2H), 2.99–2.89 (m, 1H), 2.78 (dd, J = 12.9, 6.5 Hz, 2H), 2.65–2.55 (m, 1H), 2.49 (t, J = 7.0 Hz, 3H), 2.04 (t, J = 7.0 Hz, 3H), 1.73–1.64 (m, 2H), 1.53–1.45 (m, 2H), 1.44–1.35 (m, 2H). ^{13}C NMR (126 MHz, DMSO-d_6) δ 173.34, 172.29, 171.46, 168.16, 164.87, 155.15, 145.70, 144.40, 140.20, 139.84, 138.33, 137.24, 134.40, 132.45, 129.12, 129.04, 127.37, 126.62, 124.78, 123.12, 121.74, 119.23, 96.26, 77.09, 52.11, 47.50, 42.87, 38.03, 35.32, 31.72, 29.25, 28.70, 22.91, 22.82, 16.94. HRMS (ESI, positive): Calcd. for $C_{40}H_{41}N_8O_7S$ $[M+H]^+$: m/z = 777.2813; Found: 777.2819. HPLC t_R = 13.72 min (purity 93.6 %)

3-Amino-6-(4-(N-(8-((3-(2-(2,6-dioxopiperidin-3-yl)-1-oxoisoindolin-4-yl)prop-2-yn-1-yl)amino)-8-oxooctyl)sulfamoyl)phenyl)-N-phenylpyrazine-2-carboxamide 42l. ^{1}H NMR (400 MHz, DMSO-d_6) δ 10.98 (s, 1H), 10.40 (s, 1H), 8.98 (s, 1H), 8.42 (d, J = 8.5 Hz, 2H), 8.29 (t, J = 5.2 Hz, 1H), 7.88–7.75 (m, 6H), 7.72 (d, J = 7.5 Hz, 1H), 7.61 (dd, J = 11.0, 6.6 Hz, 2H), 7.51 (t, J = 7.6 Hz, 1H), 7.38 (t, J = 7.9 Hz, 2H), 7.15 (t, J = 7.4 Hz, 1H), 5.13 (dd, J = 13.3, 5.1 Hz, 1H), 4.42 (d, J = 17.7 Hz, 1H), 4.29 (d, J = 17.8 Hz, 1H), 4.12 (d, J = 5.3 Hz, 2H), 2.95–2.84 (m, 1H), 2.72 (dd, J = 12.8, 6.6 Hz, 2H), 2.62–2.53 (m, 1H), 2.45–2.29 (m, 1H), 2.10–1.93 (m, 3H), 1.49–1.41 (m, 2H), 1.38–1.30 (m, 2H), 1.26–1.09 (m, 6H). ^{13}C NMR (101 MHz, DMSO-d_6) δ 173.23, 172.42, 171.39, 167.96, 164.82, 155.09, 145.63, 144.38, 140.16, 139.77, 138.26, 137.17, 134.57, 132.46, 129.11, 129.05, 127.31, 126.55, 124.76, 124.73, 123.63, 121.69, 118.34, 93.09, 77.75, 52.05, 47.31, 42.97, 35.51, 31.63, 29.41, 29.04, 28.93, 28.70, 26.37, 25.48, 22.89. HRMS (ESI, positive): Calcd. for $C_{41}H_{43}N_8O_7S$ $[M+H]^+$: m/z = 791.297; Found: 791.299. HPLC t_R = 14.14 min (purity 96.3 %).

3-Amino-6-(4-(N-(6-((5-(2-(1-methyl-2,6-dioxopiperidin-3-yl)-1-oxoisoindolin-4-yl)pent-4-yn-1-yl)amino)-6-oxohexyl)sulfamoyl)phenyl)-N-phenylpyrazine-2-carboxamide 42m. ^{1}H NMR (400 MHz, DMSO-d_6) δ 10.40 (s, 1H), 8.98 (s, 1H), 8.41 (d, J = 8.5 Hz, 2H), 7.89–7.73 (m, 7H), 7.69 (d, J = 7.5 Hz, 1H), 7.60 (t, J = 6.1 Hz, 2H),

7.49 (t, $J = 7.6$ Hz, 1H), 7.38 (t, $J = 7.9$ Hz, 2H), 7.14 (t, $J = 7.4$ Hz, 1H), 5.19 (dd, $J = 13.4$, 5.0 Hz, 1H), 4.43 (d, $J = 17.8$ Hz, 1H), 4.30 (d, $J = 17.9$ Hz, 1H), 3.16 (dd, $J = 13.0$, 6.5 Hz, 2H), 3.03–2.91 (m, 4H), 2.78–2.66 (m, 3H), 2.44 (t, $J = 7.0$ Hz, 3H), 1.98 (t, $J = 7.4$ Hz, 3H), 1.70–1.59 (m, 2H), 1.44–1.32 (m, 4H), 1.23–1.14 (m, 2H). ^{13}C NMR (101 MHz, DMSO-d_6) δ 172.37, 172.29, 171.00, 168.13, 164.81, 155.09, 145.63, 144.39, 140.10, 139.78, 138.26, 137.17, 134.36, 132.37, 129.04, 128.98, 127.31, 126.55, 124.76, 124.71, 123.10, 121.66, 119.18, 96.17, 77.07, 52.52, 47.41, 42.94, 37.95, 35.73, 31.80, 29.24, 28.60, 27.01, 26.24, 25.22, 22.04, 16.87. HRMS (ESI, positive): Calcd. for $C_{42}H_{45}N_8O_7S$ $[M+H]^+$: m/z = 805.313; Found: 805.312. HPLC t_R = 14.27 min (purity 98.9 %).

4-(5-Amino-6-(5-phenyl-1,3,4-oxadiazol-2-yl)pyrazin-2-yl)-N-(6-(4-(2-(2,6-dioxopiperi-din-3-yl)-1,3-dioxoisoindolin-5-yl)piperazin-1-yl)-6-oxohexyl)benzenesulfonamide 43a. ^{1}H NMR (400 MHz, DMSO-d_6) δ 11.05 (s, 1H), 8.99 (s, 1H), 8.30 (d, $J = 8.6$ Hz, 2H), 8.14 (dt, $J = 10.3$, 4.9 Hz, 2H), 7.89 (d, $J = 8.6$ Hz, 2H), 7.82 (br, 2H), 7.72–7.57 (m, 5H), 7.26 (d, $J = 2.1$ Hz, 1H), 7.16 (dd, $J = 8.6$, 2.2 Hz, 1H), 5.05 (dd, $J = 12.9$, 5.4 Hz, 1H), 3.54 (s, 4H), 3.48–3.34 (m, 4H), 2.94–2.80 (m, 1H), 2.77 (dd, $J = 12.9$, 6.7 Hz, 2H), 2.63–2.51 (m, 2H), 2.26 (t, $J = 7.4$ Hz, 2H), 2.04–1.95 (m, 1H), 1.49–1.33 (m, 4H), 1.30–1.17 (m, 2H). ^{13}C NMR (101 MHz, DMSO-d_6) δ 173.21, 171.16, 170.48, 167.92, 167.37, 164.40, 163.25, 155.22, 153.24, 144.21, 140.41, 139.88, 138.58, 134.25, 132.86, 129.98, 127.59, 127.39, 126.20, 125.31, 123.46, 120.18, 118.89, 118.11, 108.27, 49.23, 47.20, 46.94, 44.47, 42.91, 32.49, 31.43, 29.26, 26.22, 24.60, 22.62. HRMS (ESI, positive): Calcd. for $C_{41}H_{41}N_{10}O_8S$ $[M+H]^+$: m/z = 833.282; Found: 833.283. HPLC t_R = 13.52 min (purity 99.7 %).

4-(5-Amino-6-(5-phenyl-1,3,4-oxadiazol-2-yl)pyrazin-2-yl)-N-(5-(4-(2-(2,6-dioxopiperi-din-3-yl)-1,3-dioxoisoindolin-5-yl)piperazin-1-yl)-5-oxopentyl)benzenesulfonamide 43b. ^{1}H NMR (400 MHz, DMSO-d_6) δ 11.05 (s, 1H), 8.98 (s, 1H), 8.29 (d, $J = 8.5$ Hz, 2H), 8.18–8.09 (m, 2H), 7.89 (d, $J = 8.5$ Hz, 2H), 7.81 (br, 2H), 7.73–7.54 (m, 5H), 7.22 (d, $J = 1.9$ Hz, 1H), 7.12 (dd, $J = 8.6$, 2.1 Hz, 1H), 5.05 (dd, $J = 12.9$, 5.4 Hz, 1H), 3.53 (s, 4H), 3.45–3.32 (m, 4H), 2.94–2.75 (m, 3H), 2.63–2.50 (m, 2H), 2.25 (t, $J = 7.0$ Hz, 2H), 2.07–1.96 (m, 1H), 1.52–1.36 (m, 4H). ^{13}C NMR (101 MHz, DMSO-d_6) δ 173.21, 171.04, 170.48, 167.88, 167.35, 164.38, 163.22, 155.16, 153.22, 144.17, 140.40, 139.87, 138.54, 134.22, 132.84, 129.96, 127.59, 127.36, 126.17, 125.26, 123.44, 120.16, 118.88, 118.02, 108.19, 55.34, 49.22, 47.17, 46.91, 44.45, 42.79, 32.01, 31.43, 29.03, 22.63, 22.19. HRMS (ESI, positive): Calcd. for $C_{40}H_{39}N_{10}O_8S$ $[M+H]^+$: m/z = 819.267; Found: 819.269. HPLC t_R = 13.11 min (purity 99.7 %).

4-(5-Amino-6-(5-(4-((methylamino)methyl)phenyl)-1,3,4-oxadiazol-2-yl)pyrazin-2-yl)-N-(5-(4-(2-(2,6-dioxopiperidin-3-yl)-1,3-dioxoisoindolin-5-yl)piperazin-1-yl)-5-oxopentyl)benzenesulfonamide 43c. ^{1}H NMR (400 MHz, DMSO-d_6) δ 11.02 (br, 1H), 9.01 (s, 1H), 8.32 (d, $J = 8.3$ Hz, 2H), 8.10 (d, $J = 8.0$ Hz, 2H), 7.92 (d, $J = 8.4$ Hz, 2H), 7.83 (br, 2H), 7.71–7.53 (m, 4H), 7.25 (s, 1H), 7.16 (d, $J = 8.6$ Hz, 1H), 5.07 (dd, $J = 12.9$, 5.4 Hz, 1H), 3.80 (s, 2H), 3.55 (s, 4H), 3.48–3.35 (m, 4H), 2.95–2.77 (m, 3H), 2.64–2.52 (m, 2H), 2.32 (s, 3H), 2.28 (t, $J = 7.1$ Hz, 2H), 2.08–1.99 (m, 1H), 1.55–1.38 (m, 4H). ^{13}C NMR (101 MHz, DMSO-d_6) δ 173.23, 171.06, 170.50, 167.91, 167.38, 164.46, 163.12, 155.20, 153.24, 144.16, 140.43, 139.91, 138.56, 134.25, 129.46, 127.62, 127.29, 126.21, 125.29, 121.85, 120.24, 118.91, 118.06, 108.23, 54.85, 49.25, 47.21, 46.94, 46.17, 44.49, 42.82, 35.82, 32.04, 31.45, 29.05, 22.64, 22.21. HRMS (ESI, positive): Calcd. for $C_{42}H_{44}N_{11}O_8S$ $[M+H]^+$: m/z = 862.309; Found: 862.309. HPLC t_R = 10.62 min (purity 97.5 %).

1-(4-(5-(3-Amino-6-(4-(N-(6-(4-(2-(2,6-dioxopiperidin-3-yl)-1,3-dioxoisoindolin-5-yl)piperazin-1-yl)-6-oxohexyl)sulfamoyl)phenyl)pyrazin-2-yl)-1,3,4-oxadiazol-2-yl)phenyl)-N-methylmethanaminium formate 43d. ^{1}H NMR (400 MHz, DMSO-d_6) δ 11.04 (br, 1H), 9.00 (s, 1H), 8.30 (d, $J = 8.6$ Hz, 2H), 8.21–8.16 (m, 3H), 7.89 (d, $J = 8.6$ Hz, 2H), 7.83 (br, 2H), 7.70 (d, $J = 8.3$ Hz, 2H), 7.64 (d, $J = 8.5$ Hz, 2H), 7.26 (d, $J = 2.1$ Hz, 1H), 7.16 (dd, $J = 8.7$, 2.2 Hz, 1H), 5.05 (dd, $J = 12.9$, 5.4 Hz, 1H), 4.14 (s, 2H), 3.54 (s, 4H), 3.47–3.35 (m, 4H), 2.93–2.73 (m, 3H), 2.62–2.50 (m, 5H), 2.26 (t, $J = 7.4$ Hz, 2H), 2.04–1.95 (m, 1H), 1.46–1.34 (m, 4H), 1.30–1.18 (m, 2H). ^{13}C NMR (101 MHz, DMSO-d_6) δ 173.21, 171.17, 170.48, 167.92, 167.37, 164.13, 163.33, 155.21, 153.27, 144.29, 140.42, 139.85, 138.90, 138.60, 134.25, 130.84, 127.62, 127.59, 126.22, 125.31, 123.40, 120.10, 118.89, 118.11, 108.25, 52.14, 49.23, 47.19, 46.93, 44.47, 42.91, 33.47, 32.49, 31.43, 29.26, 26.22, 24.60, 22.62. HRMS (ESI, positive): Calcd. for $C_{43}H_{46}N_{11}O_8S$ $[M+H]^+$: m/z = 876.325; Found: 876.325. HPLC t_R = 9.92 min (purity 99.2 %).

1-(4-(5-(3-Amino-6-(4-(N-(7-(4-(2-(2,6-dioxopiperidin-3-yl)-1,3-dioxoisoindolin-5-yl)piperazin-1-yl)-7-oxoheptyl)sulfamoyl)phenyl)pyrazin-2-yl)-1,3,4-oxadiazol-2-yl)phenyl)-N-methylmethanaminium formate 43e. ^{1}H NMR (400 MHz, DMSO-d_6) δ 11.02 (br, 1H), 8.99 (s, 1H), 8.29 (d, $J = 8.5$ Hz, 2H), 8.26 (s, 1H), 8.13 (d, $J = 8.2$ Hz, 2H), 7.89 (d, $J = 8.5$ Hz, 2H), 7.83 (br, 2H), 7.65 (d, $J = 8.5$ Hz, 4H), 7.27 (d, $J = 1.9$ Hz, 1H), 7.17 (dd, $J = 8.7$, 2.1 Hz, 1H), 5.05 (dd, $J = 12.9$, 5.4 Hz, 1H), 3.95 (s, 2H), 3.54 (d, $J = 5.4$ Hz, 4H), 3.41 (d, $J = 19.9$ Hz, 4H), 2.93–2.80 (m, 1H), 2.77 (t, $J = 6.7$ Hz, 2H), 2.62–2.50 (m, 2H), 2.41 (s, 3H), 2.26 (t, $J = 7.4$ Hz, 2H), 2.05–1.95 (m, 1H), 1.47–1.31 (m, 4H), 1.27–1.12 (m, 4H). ^{13}C NMR (101 MHz, DMSO-d_6) δ 173.10, 171.12, 170.37, 167.81, 167.27, 164.69, 164.19, 163.12, 155.12, 153.13, 144.11, 142.08, 140.30, 139.76, 138.48, 134.14, 130.06, 127.48, 127.32, 126.10, 125.20, 122.49, 120.05, 118.78, 118.03, 108.18, 53.23, 49.13, 47.11, 46.84, 44.36, 42.85, 34.36, 32.42, 31.33, 29.21, 28.57, 26.19, 24.84, 22.52. HRMS (ESI, positive): Calcd. for $C_{44}H_{48}N_{11}O_8S$ $[M+H]^+$: m/z = 890.340; Found: 890.340. HPLC t_R = 10.27 min (purity 99.9 %).

3-Amino-6-(4-(N-(2-(2-(3-(4-(2-(2,6-dioxopiperidin-3-yl)-1,3-dioxoisoindolin-5-yl)piperazin-1-yl)-3-oxopropoxy)ethoxy)ethyl)sulfamoyl)phenyl)-N-phenylpyrazine-2-carboxamide 43f. ^{1}H NMR (400 MHz, DMSO-d_6) δ 11.05 (s, 1H), 10.39 (s, 1H), 8.98 (s, 1H), 8.41 (d, $J = 8.6$ Hz, 2H), 7.91–7.70 (m, 7H), 7.65 (d, $J = 8.5$ Hz, 1H), 7.38 (t, $J = 7.9$ Hz, 2H), 7.29 (d, $J = 2.0$ Hz, 1H), 7.21–7.11 (m, 2H), 5.05 (dd, $J = 12.9$, 5.4 Hz, 1H), 3.64–3.52 (m, 6H), 3.51–3.34 (m, 10H), 2.96–2.80 (m, 3H), 2.62–2.50 (m, 4H), 2.04–1.96 (m, 1H). ^{13}C NMR (101 MHz, DMSO-d_6) δ 173.20, 170.48, 169.47, 167.93, 167.39, 164.79, 155.23, 155.08, 145.64, 140.20, 139.82, 138.25, 137.17, 134.27, 129.05, 127.33, 126.53, 125.32, 124.75, 124.71, 121.65, 118.89, 118.13, 108.30, 70.00, 69.50, 67.12, 49.23, 47.17, 46.89, 44.57, 42.82, 40.79, 33.23, 31.43, 22.62. HRMS (ESI, positive): Calcd. for $C_{41}H_{44}N_9O_{10}S$ $[M+H]^+$: m/z = 854.293; Found: 854.292. HPLC t_R = 13.04 min (purity 99.8 %).

3-Amino-6-(4-(N-(2-(2-(2-(3-(4-(2-(2,6-dioxopiperidin-3-yl)-1,3-dioxoisoindolin-5-yl)piperazin-1-yl)-3-oxopropoxy)ethoxy)ethyl)sulfamoyl)phenyl)-N-phenyl-pyrazine-2-carboxamide 43g. ^{1}H NMR (400 MHz, DMSO-d_6) δ 11.05 (s, 1H), 10.39 (s, 1H), 8.98 (s, 1H), 8.41 (d, $J = 8.6$ Hz, 2H), 7.89–7.71 (m, 7H), 7.66 (d, $J = 8.5$ Hz, 1H), 7.38 (t, $J = 7.9$ Hz, 2H), 7.29 (d, $J = 2.0$ Hz, 1H), 7.21–7.11 (m, 2H), 5.05 (dd, $J = 12.9$, 5.4 Hz, 1H), 3.64–3.53 (m, 6H), 3.52–3.34 (m, 14H), 2.91 (q, $J = 5.8$ Hz, 2H), 2.88–2.80 (m, 1H), 2.62–2.50 (m, 4H), 2.04–1.96 (m, 1H). ^{13}C NMR (101 MHz, DMSO-d_6) δ 173.21, 170.48, 169.50, 167.94, 167.39, 164.79, 155.24, 155.08, 145.64, 140.20, 139.81, 138.25, 137.17, 134.27, 129.05, 127.33, 126.53, 125.32, 124.74, 124.72, 121.65, 118.89, 118.13, 108.30, 70.19, 70.09, 70.03, 69.50, 67.16, 49.24, 47.19, 46.89, 44.60, 42.81, 40.80, 33.24, 31.43, 22.62. HRMS (ESI, positive): Calcd. for $C_{43}H_{47}N_9NaO_{11}S$ $[M+Na]^+$: m/z = 920.301; Found: 920.302. HPLC t_R = 13.16 min (purity 98.8 %).

3-Amino-6-(4-(N-(6-(4-(2-(2,6-dioxopiperidin-3-yl)-1,3-dioxoisoindolin-5-yl)piperazin-1-yl)-6-oxohexyl)sulfamoyl)phenyl)-N-phenylpyrazine-2-carboxamide 43h. ^{1}H NMR (400 MHz, DMSO-d_6) δ 11.05 (s, 1H), 10.39 (s, 1H), 8.98 (s, 1H), 8.42 (d, $J = 8.5$ Hz, 2H), 7.92–7.72 (m, 6H), 7.69–7.58 (m, 2H), 7.38 (t, $J = 7.9$ Hz, 2H), 7.29 (d, $J = 1.9$ Hz, 1H), 7.23–7.09 (m, 2H), 5.05 (dd, $J = 12.9$, 5.4 Hz, 1H), 3.54 (s, 4H), 3.42 (d, $J = 16.1$ Hz, 4H), 2.93–2.79 (m, 1H), 2.75 (dd, $J = 12.9$,

6.7 Hz, 2H), 2.63–2.51 (m, 2H), 2.26 (t, J = 7.3 Hz, 2H), 2.04–1.93 (m, 1H), 1.49–1.32 (m, 4H), 1.30–1.17 (m, 2H). ^{13}C NMR (101 MHz, DMSO-d_6) δ 173.21, 171.17, 170.48, 167.94, 167.39, 164.80, 155.25, 155.08, 145.64, 140.18, 139.77, 138.25, 137.16, 134.27, 129.05, 127.32, 126.56, 125.34, 124.75, 124.72, 121.67, 118.91, 108.31, 49.24, 47.21, 46.95, 44.47, 42.91, 32.49, 31.42, 29.27, 26.24, 24.60, 22.62. HRMS (ESI, positive): Calcd. for $C_{40}H_{42}N_9O_8S$ $[M+H]^+$: m/z = 808.287; Found: 808.288. HPLC t_R = 13.24 min (purity 98.3 %).

3-Amino-6-(4-(N-(7-(4-(2-(2,6-dioxopiperidin-3-yl)-1,3-dioxoisoindolin-5-yl)piperazin-1-yl)-7-oxoheptyl)sulfamoyl)phenyl)-N-phenylpyrazine-2-carboxamide 43i. ^{1}H NMR (400 MHz, DMSO-d_6) δ 11.05 (s, 1H), 10.39 (s, 1H), 8.98 (s, 1H), 8.42 (d, J = 8.5 Hz, 2H), 7.93–7.72 (m, 6H), 7.66 (d, J = 8.5 Hz, 1H), 7.61 (t, J = 5.7 Hz, 1H), 7.38 (t, J = 7.9 Hz, 2H), 7.30 (d, J = 1.9 Hz, 1H), 7.23–7.10 (m, 2H), 5.05 (dd, J = 12.9, 5.4 Hz, 1H), 3.55 (s, 4H), 3.43 (d, J = 19.3 Hz, 4H), 2.93–2.80 (m, 1H), 2.75 (dd, J = 13.0, 6.7 Hz, 2H), 2.61–2.50 (m, 2H), 2.26 (t, J = 7.4 Hz, 2H), 2.04–1.95 (m, 1H), 1.47–1.31 (m, 4H), 1.26–1.13 (m, 4H). ^{13}C NMR (101 MHz, DMSO-d_6) δ 173.20, 171.23, 170.48, 167.94, 167.39, 164.80, 155.26, 155.08, 145.64, 140.20, 139.77, 138.25, 137.16, 134.27, 129.05, 127.32, 126.55, 125.33, 124.75, 121.66, 118.91, 118.16, 108.33, 55.34, 49.24, 47.22, 46.96, 44.47, 42.95, 32.53, 31.43, 29.29, 28.68, 26.31, 24.95, 22.62. HRMS (ESI, positive): Calcd. for $C_{41}H_{44}N_9O_8S$ $[M+H]^+$: m/z = 822.303; Found: 822.303. HPLC t_R = 13.61 min (purity 98.7 %).

3-Amino-6-(4-(N-(5-(4-(2-(2,6-dioxopiperidin-3-yl)-1,3-dioxoisoindolin-5-yl)piperazin-1-yl)-5-oxopentyl)sulfamoyl)phenyl)-N-phenylpyrazine-2-carboxamide 43j. ^{1}H NMR (400 MHz, DMSO-d_6) δ 11.05 (s, 1H), 10.38 (s, 1H), 8.98 (s, 1H), 8.42 (d, J = 8.5 Hz, 2H), 7.91–7.73 (m, 6H), 7.64 (dd, J = 10.1, 4.3 Hz, 2H), 7.38 (t, J = 7.9 Hz, 2H), 7.28 (d, J = 1.9 Hz, 1H), 7.20–7.11 (m, 2H), 5.05 (dd, J = 12.9, 5.4 Hz, 1H), 3.54 (s, 4H), 3.41 (d, J = 18.3 Hz, 4H), 2.92–2.74 (m, 3H), 2.61–2.50 (m, 2H), 2.26 (t, J = 7.0 Hz, 2H), 2.04–1.95 (m, 1H), 1.52–1.37 (m, 4H). ^{13}C NMR (101 MHz, DMSO-d_6) δ 173.21, 171.05, 170.49, 167.93, 167.38, 164.78, 155.22, 155.07, 145.63, 140.17, 139.77, 138.24, 137.14, 134.26, 129.04, 127.33, 126.55, 125.32, 124.73, 121.66, 118.92, 118.11, 108.29, 55.33, 49.23, 47.19, 46.93, 44.46, 42.82, 32.03, 31.42, 29.06, 22.62, 22.22. HRMS (ESI, positive): Calcd. for $C_{39}H_{39}N_9NaO_8S$ $[M+Na]^+$: m/z = 816.254; Found: 816.254. HPLC t_R = 13.17 min (purity 97.7 %).

3-Amino-6-(4-(N-(8-(4-(2-(2,6-dioxopiperidin-3-yl)-1,3-dioxoisoindolin-5-yl)piperazin-1-yl)-8-oxooctyl)sulfamoyl)phenyl)-N-phenylpyrazine-2-carboxamide 43k. ^{1}H NMR (400 MHz, DMSO-d_6) δ 11.05 (s, 1H), 10.40 (s, 1H), 8.98 (s, 1H), 8.42 (d, J = 8.5 Hz, 2H), 7.91–7.73 (m, 6H), 7.67 (d, J = 8.5 Hz, 1H), 7.61 (t, J = 5.7 Hz, 1H), 7.38 (t, J = 7.9 Hz, 2H), 7.30 (d, J = 1.9 Hz, 1H), 7.23–7.11 (m, 2H), 5.05 (dd, J = 12.9, 5.4 Hz, 1H), 3.55 (s, 4H), 3.43 (d, J = 18.2 Hz, 4H), 2.92–2.82 (m, 1H), 2.75 (dd, J = 12.9, 6.7 Hz, 2H), 2.62–2.51 (m, 2H), 2.26 (t, J = 7.4 Hz, 2H), 2.04–1.96 (m, 1H), 1.48–1.30 (m, 4H), 1.25–1.13 (m, 6H). ^{13}C NMR (101 MHz, DMSO-d_6) δ 173.21, 171.26, 170.48, 167.94, 167.39, 164.80, 155.27, 155.08, 145.63, 140.22, 139.76, 138.25, 137.17, 134.27, 129.05, 127.32, 126.54, 125.34, 124.74, 121.66, 118.90, 118.16, 108.33, 49.24, 47.22, 46.96, 44.49, 42.96, 32.60, 31.43, 29.35, 29.08, 28.80, 26.37, 25.00, 22.63. HRMS (ESI, positive): Calcd. for $C_{42}H_{46}N_9O_8S$ $[M+H]^+$: m/z = 836.318; Found: 836.320. HPLC t_R = 14.36 min (purity 96.4 %).

3-Amino-6-(4-(N-(7-((2-(4-(2,6-dioxopiperidin-3-yl)phenoxy)ethyl)amino)-7-oxoheptyl)sulfamoyl)phenyl)-N-phenylpyrazine-2-carboxamide 44a. ^{1}H NMR (400 MHz, DMSO-d_6) δ 10.75 (s, 1H), 10.40 (s, 1H), 8.98 (s, 1H), 8.42 (d, J = 8.5 Hz, 2H), 7.95 (t, J = 5.4 Hz, 1H), 7.90–7.72 (m, 6H), 7.59 (t, J = 5.8 Hz, 1H), 7.38 (t, J = 7.9 Hz, 2H), 7.15 (t, J = 7.4 Hz, 1H), 7.09 (d, J = 8.6 Hz, 2H), 6.85 (d, J = 8.6 Hz, 2H), 3.91 (t, J = 5.7 Hz, 2H), 3.75 (dd, J = 11.3, 4.9 Hz, 1H), 3.35 (dd, J = 11.2, 5.6 Hz, 2H), 2.72 (dd, J = 13.0, 6.7 Hz, 2H), 2.67–2.56 (m, 1H), 2.46–2.40 (m, 1H), 2.18–2.07 (m, 1H), 2.05–1.93 (m, 3H), 1.46–1.27 (m, 4H), 1.25–1.09 (m, 4H). ^{13}C NMR (101 MHz, DMSO-d_6) δ 174.85, 173.84, 172.84, 164.82, 157.75, 155.09, 145.64, 140.16, 139.77, 138.27, 137.18, 131.61, 129.98, 129.05, 127.31, 126.56, 124.76, 124.72, 121.67, 114.74, 66.76, 46.93, 42.98, 38.57, 35.61, 31.78, 29.29, 28.57, 26.43, 26.25, 25.53. HRMS (ESI, positive): Calcd. for $C_{37}H_{41}N_7NaO_7S$ $[M+Na]^+$: m/z = 750.269; Found: 750.270. HPLC t_R = 13.34 min (purity 97.6 %).

3-Amino-6-(4-(N-(5-((2-(4-(2,6-dioxopiperidin-3-yl)phenoxy)ethyl)amino)-5-oxopentyl)sulfamoyl)phenyl)-N-phenylpyrazine-2-carboxamide 44b. ^{1}H NMR (400 MHz, DMSO-d_6) δ 10.75 (s, 1H), 10.41 (s, 1H), 8.98 (s, 1H), 8.42 (d, J = 8.5 Hz, 2H), 7.97 (t, J = 5.5 Hz, 1H), 7.90–7.72 (m, 6H), 7.62 (t, J = 5.8 Hz, 1H), 7.38 (t, J = 7.9 Hz, 2H), 7.15 (t, J = 7.4 Hz, 1H), 7.09 (d, J = 8.6 Hz, 2H), 6.85 (d, J = 8.6 Hz, 2H), 3.91 (t, J = 5.7 Hz, 2H), 3.75 (dd, J = 11.3, 4.9 Hz, 1H), 3.35 (dd, J = 11.3, 5.7 Hz, 2H), 2.73 (dd, J = 13.0, 6.6 Hz, 2H), 2.65–2.57 (m, 1H), 2.47–2.39 (m, 1H), 2.17–2.06 (m, 1H), 2.06–1.92 (m, 3H), 1.51–1.41 (m, 2H), 1.40–1.29 (m, 2H). ^{13}C NMR (101 MHz, DMSO-d_6) δ 174.85, 173.84, 172.60, 164.82, 157.73, 155.09, 145.65, 140.12, 139.77, 138.27, 137.19, 131.62, 129.98, 129.06, 127.31, 126.57, 124.76, 124.73, 121.67, 114.75, 66.75, 46.93, 42.81, 38.57, 35.11, 31.78, 29.11, 26.42, 22.83. HRMS (ESI, positive): Calcd. for $C_{35}H_{38}N_7O_7S$ $[M+H]^+$: m/z = 700.255; Found: 700.255. HPLC t_R = 13.18 min (purity 99.7 %).

3-Amino-6-(4-(N-(8-((2-(4-(2,6-dioxopiperidin-3-yl)phenoxy)ethyl)amino)-8-oxooctyl)sulfamoyl)phenyl)-N-phenylpyrazine-2-carboxamide 44c. ^{1}H NMR (400 MHz, DMSO-d_6) δ 10.76 (s, 1H), 10.41 (s, 1H), 8.98 (s, 1H), 8.42 (d, J = 8.6 Hz, 2H), 7.95 (t, J = 5.4 Hz, 1H), 7.90–7.74 (m, 6H), 7.60 (t, J = 5.8 Hz, 1H), 7.41–7.35 (m, 2H), 7.18–7.12 (m, 1H), 7.09 (d, J = 8.7 Hz, 2H), 6.86 (d, J = 8.7 Hz, 2H), 3.92 (t, J = 5.7 Hz, 2H), 3.75 (dd, J = 11.3, 4.9 Hz, 1H), 3.36 (q, J = 5.6 Hz, 2H), 2.72 (dd, J = 13.0, 6.8 Hz, 2H), 2.68–2.56 (m, 1H), 2.47–2.39 (m, 1H), 2.18–2.06 (m, 1H), 2.05–1.91 (m, 3H), 1.49–1.38 (m, 2H), 1.37–1.29 (m, 2H), 1.23–1.10 (m, 6H). ^{13}C NMR (101 MHz, DMSO-d_6) δ 174.84, 173.84, 172.87, 164.82, 157.76, 155.09, 145.63, 140.18, 139.77, 138.27, 137.18, 131.61, 129.98, 129.05, 127.31, 126.55, 124.76, 124.72, 121.67, 114.74, 66.77, 46.93, 42.99, 38.58, 35.68, 31.78, 29.42, 28.94, 28.73, 26.44, 26.38, 25.57. HRMS (ESI, positive): Calcd. for $C_{38}H_{44}N_7O_7S$ $[M+H]^+$: m/z = 742.302; Found: 742.302. HPLC t_R = 14.05 min (purity 98.4 %).

3-Amino-6-(4-(N-(6-(4-(6-((2,6-dioxopiperidin-3-yl)carbamoyl)pyridin-2-yl)piperazin-1-yl)-6-oxohexyl)sulfamoyl)phenyl)-N-phenylpyrazine-2-carboxamide 44d. ^{1}H NMR (400 MHz, DMSO-d_6) δ 10.86 (s, 1H), 10.40 (s, 1H), 8.98 (s, 1H), 8.75 (d, J = 8.4 Hz, 1H), 8.42 (d, J = 8.3 Hz, 2H), 7.93–7.54 (m, 8H), 7.38 (t, J = 7.7 Hz, 2H), 7.32 (d, J = 7.2 Hz, 1H), 7.15 (t, J = 7.3 Hz, 1H), 7.01 (d, J = 8.6 Hz, 1H), 4.78–4.66 (m, 1H), 3.67–3.41 (m, 8H), 2.87–2.66 (m, 3H), 2.58–2.50 (m, 1H), 2.35–2.15 (m, 3H), 1.97 (dd, J = 8.5, 3.4 Hz, 1H), 1.49–1.33 (m, 4H), 1.31–1.19 (m, 2H). ^{13}C NMR (101 MHz, DMSO-d_6) δ 173.44, 172.69, 171.12, 164.81, 164.58, 158.00, 155.08, 147.89, 145.64, 140.15, 139.78, 139.28, 138.26, 137.17, 129.05, 127.32, 126.57, 124.76, 124.72, 121.68, 111.79, 110.78, 49.88, 45.11, 44.92, 44.72, 42.92, 41.05, 32.57, 31.46, 29.32, 26.29, 24.71, 24.49. HRMS (ESI, positive): Calcd. for $C_{38}H_{43}N_{10}O_7S$ $[M+H]^+$: m/z = 783.3031; Found: 783.3027. HPLC t_R = 13.23 min (purity 95.2 %).

3-Amino-6-(4-(N-(2-(2-(3-(((*S*)-1-((2*S*,4*R*)-4-hydroxy-2-((4-(4-methylthiazol-5-yl)benzyl)carbamoyl)pyrrolidin-1-yl)-3,3-dimethyl-1-oxobutan-2-yl)amino)-3-oxoprop-oxy)ethoxy)ethyl)sulfamoyl)phenyl)-N-phenylpyrazine-2-carboxamide 45a. ^{1}H NMR (400 MHz, DMSO-d_6) δ 10.41 (s, 1H), 8.98 (s, 1H), 8.95 (s, 1H), 8.52 (t, J = 6.0 Hz, 1H), 8.41 (d, J = 8.5 Hz, 2H), 7.92–7.71 (m, 8H), 7.45–7.32 (m, 6H), 7.14 (t, J = 7.4 Hz, 1H), 5.09 (d, J = 3.5 Hz, 1H), 4.52 (d, J = 9.4 Hz, 1H), 4.46–4.28 (m, 3H), 4.20 (dd, J = 15.8, 5.5 Hz, 1H), 3.68–3.50 (m, 4H), 3.48–3.34 (m, 6H), 2.91 (dd, J = 11.7, 5.8 Hz, 2H), 2.56–2.49 (m, 1H), 2.42 (s, 3H), 2.36–2.25 (m, 1H), 2.07–1.95 (m, 1H), 1.93–1.83 (m, 1H), 0.89 (s, 9H). ^{13}C NMR (101 MHz, DMSO-d_6) δ 172.32, 170.35, 169.96, 164.81, 155.09, 151.84, 148.15, 145.64, 140.17, 139.92, 139.83, 138.26, 137.19, 131.59, 130.09, 129.07, 129.05, 127.86, 127.33, 126.54, 124.77, 124.72, 121.68, 69.98, 69.78,

69.54, 69.31, 67.35, 59.14, 56.73, 42.79, 42.10, 38.38, 36.08, 35.78, 26.75, 16.38. HRMS (ESI, positive): Calcd. for $C_{46}H_{55}N_9NaO_9S_2$ $[M+Na]^+$: m/z = 964.346; Found: 964.347. HPLC t_R = 14.39 min (purity 100 %).

3-Amino-6-(4-(N-((S)-14-((2S,4R)-4-hydroxy-2-((4-(4-methylthiazol-5-yl)benzyl)carbamoyl)pyrrolidine-1-carbonyl)-15,15-dimethyl-12-oxo-3,6,9-trioxa-13-azahexadecyl)sulfamoyl)phenyl)-N-phenylpyrazine-2-carboxamide 45b. ^{1}H NMR (400 MHz, DMSO-d_6) δ 10.40 (s, 1H), 8.98 (s, 1H), 8.95 (s, 1H), 8.52 (t, J = 5.9 Hz, 1H), 8.41 (d, J = 8.6 Hz, 2H), 7.91–7.72 (m, 8H), 7.44–7.33 (m, 6H), 7.14 (t, J = 7.4 Hz, 1H), 5.09 (br, 1H), 4.53 (d, J = 9.4 Hz, 1H), 4.46–4.28 (m, 3H), 4.20 (dd, J = 15.8, 5.4 Hz, 1H), 3.69–3.51 (m, 4H), 3.49–3.37 (m, 10H), 2.91 (q, J = 5.8 Hz, 2H), 2.55–2.49 (m, 1H), 2.42 (s, 3H), 2.36–2.27 (m, 1H), 2.06–1.97 (m, 1H), 1.93–1.83 (m, 1H), 0.90 (s, 9H). ^{13}C NMR (101 MHz, DMSO-d_6) δ 172.33, 170.35, 169.97, 164.81, 155.09, 151.84, 148.15, 145.64, 140.19, 139.93, 139.82, 138.27, 137.19, 131.59, 130.08, 129.07, 129.05, 127.86, 127.33, 126.55, 124.77, 124.72, 121.67, 70.13, 70.10, 70.03, 69.89, 69.54, 69.31, 67.37, 59.15, 56.80, 56.74, 42.80, 42.10, 38.38, 36.10, 35.79, 26.76, 16.37. HRMS (ESI, positive): Calcd. for $C_{48}H_{59}N_9NaO_{10}S_2$ $[M+Na]^+$: m/z = 1008.372; Found: 1008.374. HPLC t_R = 14.43 min (purity 99.6 %).

3-Amino-6-(4-(N-(6-(((S)-1-((2S,4R)-4-hydroxy-2-((4-(4-methylthiazol-5-yl)benzyl)carbamoyl)pyrrolidin-1-yl)-3,3-dimethyl-1-oxobutan-2-yl)amino)-6-oxohexyl)sulfamoyl)phenyl)-N-phenylpyrazine-2-carboxamide 45c. ^{1}H NMR (400 MHz, DMSO-d_6) δ 10.41 (s, 1H), 8.98 (s, 1H), 8.95 (s, 1H), 8.51 (t, J = 6.0 Hz, 1H), 8.42 (d, J = 8.5 Hz, 2H), 7.89–7.73 (m, 7H), 7.60 (t, J = 5.7 Hz, 1H), 7.43–7.31 (m, 6H), 7.14 (t, J = 7.4 Hz, 1H), 5.08 (d, J = 3.5 Hz, 1H), 4.50 (d, J = 9.4 Hz, 1H), 4.46–4.29 (m, 3H), 4.19 (dd, J = 15.8, 5.4 Hz, 1H), 3.68–3.56 (m, 2H), 2.72 (dd, J = 13.0, 6.8 Hz, 2H), 2.42 (s, 3H), 2.27–2.14 (m, 1H), 2.12–1.96 (m, 2H), 1.93–1.83 (m, 1H), 1.46–1.31 (m, 4H), 1.26–1.16 (m, 2H), 0.89 (s, 9H). ^{13}C NMR (101 MHz, DMSO-d_6) δ 172.38, 172.35, 170.13, 164.82, 155.09, 151.85, 148.15, 145.64, 140.10, 139.93, 139.77, 138.27, 137.18, 131.59, 130.08, 129.06, 129.05, 127.86, 127.32, 126.56, 124.77, 124.71, 121.67, 69.30, 59.12, 56.73, 42.94, 42.10, 38.38, 35.63, 35.20, 29.24, 26.81, 26.27, 25.43, 16.38. HRMS (ESI, positive): Calcd. for $C_{45}H_{54}N_9O_7S_2$ $[M+H]^+$: m/z = 896.358; Found: 896.358. HPLC t_R = 14.46 min (purity 97.9 %).

(2S,4R)-1-((S)-2-(6-((4-(5-amino-6-(5-(4-((methylamino)methyl)phenyl)-1,3,4-oxadiazol-2-yl)pyrazin-2-yl)phenyl)sulfonamido)hexanamido)-3,3-dimethylbutanoyl)-4-hydroxy-N-(4-(4-methylthiazol-5-yl)benzyl)pyrrolidine-2-carboxamide 45d. ^{1}H NMR (400 MHz, DMSO-d_6) δ 8.99 (s, 1H), 8.95 (s, 1H), 8.52 (t, J = 5.9 Hz, 1H), 8.29 (d, J = 8.5 Hz, 2H), 8.10 (d, J = 8.2 Hz, 2H), 7.95–7.73 (m, 5H), 7.61 (d, J = 8.2 Hz, 3H), 7.37 (q, J = 8.2 Hz, 4H), 5.09 (br, 1H), 4.50 (d, J = 9.4 Hz, 1H), 4.46–4.28 (m, 3H), 4.19 (dd, J = 15.9, 5.3 Hz, 1H), 3.80 (s, 2H), 3.67–3.55 (m, 2H), 2.78–2.69 (m, 2H), 2.41 (s, 3H), 2.32 (s, 3H), 2.23–2.14 (m, 1H), 2.11–1.97 (m, 2H), 1.92–1.83 (m, 1H), 1.48–1.32 (m, 4H), 1.25–1.16 (m, 2H), 0.89 (s, 9H). ^{13}C NMR (101 MHz, DMSO-d_6) δ 172.40, 172.35, 170.13, 164.45, 163.17, 153.24, 151.83, 148.14, 144.17, 140.30, 139.92, 139.88, 138.60, 131.58, 130.07, 129.57, 129.05, 127.85, 127.58, 127.31, 126.21, 121.97, 120.23, 69.30, 59.12, 56.74, 54.60, 42.94, 42.10, 38.37, 35.62, 35.59, 35.21, 29.26, 26.81, 26.26, 25.44, 16.37. HRMS (ESI, positive): Calcd. for $C_{48}H_{58}N_{11}O_7S_2$ $[M+H]^+$: m/z = 964.396; Found: 964.395. HPLC t_R = 13.37 min (purity 98.1 %).

(2S,4R)-1-((S)-2-(6-((4-(5-amino-6-(5-phenyl-1,3,4-oxadiazol-2-yl)pyrazin-2-yl)phenyl)sulfonamido)hexanamido)-3,3-dimethylbutanoyl)-4-hydroxy-N-(4-(4-methylthiazol-5-yl)benzyl)pyrrolidine-2-carboxamide 45e. ^{1}H NMR (400 MHz, DMSO-d_6) δ 8.99 (s, 1H), 8.95 (s, 1H), 8.51 (t, J = 5.9 Hz, 1H), 8.29 (d, J = 8.5 Hz, 2H), 8.15 (dd, J = 7.6, 1.7 Hz, 2H), 7.95–7.73 (m, 5H), 7.70–7.56 (m, 4H), 7.37 (q, J = 8.3 Hz, 4H), 5.08 (d, J = 3.5 Hz, 1H), 4.50 (d, J = 9.4 Hz, 1H), 4.45–4.28 (m, 3H), 4.19 (dd, J = 15.8, 5.2 Hz, 1H), 3.67–3.55 (m, 2H), 2.74 (dd, J = 13.0, 6.7 Hz, 2H), 2.41 (s, 3H), 2.24–2.14 (m, 1H), 2.11–1.96 (m, 2H), 1.92–1.83 (m, 1H), 1.45–1.32 (m, 4H), 1.25–1.16 (m, 2H), 0.89 (s, 9H). ^{13}C NMR (101 MHz, DMSO-d_6) δ 172.39, 172.35, 170.13, 164.43, 163.29, 153.25, 151.84, 148.14, 144.22, 140.31, 139.92, 139.88, 138.61, 132.86, 131.58, 130.07, 129.99, 129.05, 127.85, 127.58, 127.40, 126.21, 123.48, 120.20, 69.30, 59.12, 56.73, 42.94, 42.10, 38.37, 35.62, 35.21, 29.25, 26.80, 26.25, 25.43, 16.37. HRMS (ESI, positive): Calcd. for $C_{46}H_{53}N_{10}O_7S_2$ $[M+H]^+$: m/z = 921.353; Found: 921.354. HPLC t_R = 14.75 min (purity 99.6 %).

(2S,4R)-1-((S)-2-(5-((4-(5-amino-6-(5-phenyl-1,3,4-oxadiazol-2-yl)pyrazin-2-yl)phenyl)sulfonamido)pentanamido)-3,3-dimethylbutanoyl)-4-hydroxy-N-(4-(4-methylthiazol-5-yl)benzyl)pyrrolidine-2-carboxamide 45f. ^{1}H NMR (400 MHz, DMSO-d_6) δ 8.99 (s, 1H), 8.94 (s, 1H), 8.51 (t, J = 5.9 Hz, 1H), 8.29 (d, J = 8.5 Hz, 2H), 8.19–8.10 (m, 2H), 7.93–7.74 (m, 5H), 7.70–7.59 (m, 4H), 7.36 (q, J = 8.3 Hz, 4H), 5.08 (d, J = 3.5 Hz, 1H), 4.50 (d, J = 9.3 Hz, 1H), 4.44–4.29 (m, 3H), 4.19 (dd, J = 15.9, 5.4 Hz, 1H), 3.69–3.56 (m, 2H), 2.76 (dd, J = 12.6, 6.4 Hz, 2H), 2.41 (s, 3H), 2.26–2.13 (m, 1H), 2.13–1.96 (m, 2H), 1.92–1.83 (m, 1H), 1.51–1.32 (m, 4H), 0.89 (s, 9H). ^{13}C NMR (101 MHz, DMSO-d_6) δ 172.35, 172.23, 170.11, 164.42, 163.28, 153.25, 151.83, 148.14, 144.21, 140.36, 139.91, 139.87, 138.61, 132.85, 131.58, 130.07, 129.98, 129.05, 127.84, 127.56, 127.39, 126.20, 123.47, 120.19, 69.30, 59.12, 56.75, 42.84, 42.10, 38.37, 35.63, 34.81, 29.25, 26.81, 23.11, 16.37. HRMS (ESI, positive): Calcd. for $C_{45}H_{50}N_{10}NaO_7S_2$ $[M+Na]^+$: m/z = 929.320; Found: 929.320. HPLC t_R = 14.61 min (purity 99.8 %).

4.4. Non-enzymatic stability testing

The developed compounds were diluted in the assay media consisting of a mixture of DMEM (50 %), DMSO (10 %) and acetonitrile (40 %) at pH 7.4 and incubated at 37 °C for 72 h. The quantity of the compounds was measured after 6, 12, 24, 48, and 72 h by HPLC using an XTerra RP18 column (3.5 mm, 3.9 mm × 100 mm) from the manufacturer Waters (Milford, MA, USA) and two LC-10AD pumps, an SPD-M10AVP PDA detector, and an SIL-HT autosampler, all from the manufacturer Shimadzu (Kyoto, Japan). UV absorbance was measured at 254 nm was used. In some cases the percentage value of the compounds after 72 h-incubation increased over 100 %. This might be explained by evaporation of small amounts of solvent in the sample vials during 37 °C for 72 h.

4.5. Plasma stability and protein binding

To determine protein binding 20 μM of the given compound was incubated with 100 μL human pooled plasma (P9523, Sigma Aldrich, Darmstadt, Germany) and free amount of compound was measured after 5 min by HPLC as described below. To determine plasma stability, 20 μM of the given compound was incubated with 100 μL human pooled plasma for 5, 10, 20, 30, 60 and 120 min at 37 °C (1st run), and for 1h, 2h, 6 h, 12 h, and 24 h at 37 °C (2nd run). The reactions were stopped by adding 300 μL of acetonitrile with subsequent plasma proteins sedimentation. The samples were subjected to ultra-centrifugation (5 min, 10000 RPM/g) using modified PES 30K low protein binding centrifugal filter. The filtrate was then analyzed using HPLC to determine the available concentration of the compounds and also to determine and quantify potential degradation products. The percentage of the test compound remaining after incubation in plasma was calculated and is listed in Tables S4 and S5 in the Supplement. As HPLC system a LiChrosorb® RP-18 (5 μm) 100-4.6 column from the manufacturer Merck, two LC-10AD pumps, a SPD-M10A VP PDA detector, and a SIL-HT auto-sampler were used (all from the manufacturer Shimadzu, Kyoto, Japan). As mobile phase a gradient with increasing polarity composed of methanol/water/trifluoroacetic acid at a flow rate of 1 ml/min. UV absorbance was measured at 300 nm was used.

4.6. Cellular assay/degradation assay

4.6.1. Drugs and chemicals used as references

Bortezomib (#S1013), MG132 (#S2619), and VE-821 (#S8007) were purchased from Selleck Chemicals, Munich, Germany. Irinotecan (#I1406) was purchased from Sigma-Aldrich, Taufkirchen, Germany. Stock solutions in DMSO were stored at −80 °C. All drugs were diluted in PBS before treatment.

4.6.2. Cell lines

Human pancreatic cancer cell line MIA PaCa-2 was kindly provided by Matthias Wirth (Berlin, Germany). The human cervix cancer cell line HeLa was a gift from Roland H. Stauber (Mainz, Germany). Cells were cultured in high glucose DMEM (D5796, Sigma-Aldrich, Munich, Germany), supplemented with 10 % fetal calf serum (FCS) and 1 % (w/v) penicillin/streptomycin (Thermo Fisher, Gibco, Braunschweig, Germany). Cells were confirmed to be mycoplasma-free and were verified by DNA fingerprint at the DSMZ, Braunschweig, Germany.

4.6.3. Immunoblot

Immunoblots were carried out as described by our group [35]. Antibodies used for this assay were: ATR (#cs2790), *p*-CHK1 (S345) (#cs2348), and CRBN (cs71810) from Cell Signaling, Leiden, Netherlands; GSPT1 (#sc-515615), HSP90 (#sc-13119), and vinculin (#sc-73614) from Santa Cruz Biotechnology, Heidelberg, Germany; ATM (#ab32420) and DNA-PKcs (#ab32566) from Abcam, Cambridge, U.K.; *p*-ATR (T1989) (#GTX128145) from GeneTex, CA, USA; ubiquitin (#05–1307) from Sigma-Aldrich, Taufkirchen, Germany. HSP90 and vinculin served as independent housekeeping proteins to normalize protein loading. The protein ladder used was the PageRuler™ Plus pre-stained protein ladder (#26619) from Thermo Fischer Scientific, MA, USA.

4.6.4. RNA interference

Knock-down of CRBN in MIA PaCa-2 cells was performed by transfecting 30 pmol of siRNA against CRBN (Thermo Fischer Scientific, MA, USA, #4392420) or the same amount of non-targeting control siRNA-C (Santa Cruz Biotechnology, Heidelberg, Germany, #sc-44231) with Lipofectamine® RNAiMAX (Invitrogen, Darmstadt, Germany), according to manufacturer's protocol. After 48 h, growth media with transfection mixture was removed and cells were treated with **42i** (2 μM) and/or irinotecan (5 μM) for 24 h. Knock-down efficiency was confirmed by immunoblotting.

4.6.5. ATR/ATRIP non-radioactive in vitro assay

Measurement was done by Eurofins (Eurofins Discovery 11180 Roselle Street, Suite D, San Diego, CA 92121 USA) using the KinaseProfiler™ assay. Human ATR/ATRIP was incubated with 25 mM HEPES pH 8.0, 0.01 % Brij-35, 1 % Glycerol, 10 μM ATP, 10 mM MnCl2 and 50 nM GST-cMyc-p53. The reaction was initiated with the addition of ATP. After incubation for 30 min at room temperature, the reaction was terminated by the addition of a stop solution containing EDTA. Finally, detection buffer was added, which contained d2-labelled anti-GST monoclonal antibody, and a Europium-labelled anti-phospho Ser15 antibody against phosphorylated p53. The plate was then read in time-resolved fluorescence mode and the homogeneous time-resolved fluorescence (HTRF) signal was determined according to the formula HTRF = 10000 x (Em_{665nm}/Em_{620nm}).

4.6.6. Flow cytometry and Alamar Blue assay

Annexin-V/propidium iodine staining and flow cytometry were conducted as recently described by us [35]. In brief, adherent and floating MIA PaCa-2 cells were collected after trypsinization, washed with 1x PBS and incubated with annexin-V coupled to the dye FITC (Miltenyi Biotec, Bergisch Gladbach, Germany) plus PI (Sigma-Aldrich, Munich, Germany). Analyses were done with a FACS Canto II (BD Bioscience, Heidelberg, Germany) and the software tool FACSDiva 7.0. To determine the cytotoxicity on human epithelial kidney cells, we used HEK293 cells (DSMZ Braunschweig, ACC305). These were incubated at 37 °C in a humidified incubator with 5 % CO_2 in DMEM supplemented with 10 % FCS and 5 mM glutamine. Cells were seeded out at 1.5 x 10^3 cells per well in a 96-well cell culture plate (TPP, Switzerland). The compounds to be tested were added immediately to the medium at 50 μM. After 24 h, Alamar Blue reagent (Invitrogen, CA) was added and incubated again for 21 h before samples were analyzed. Detection of viable cells which convert the resazurine reagent into the highly fluorescent resorufin was performed by using a FLUOstarOPTIMA microplate reader (BMG Labtec) using the following filter set: Ex 530 nm/Em 590 nm. All measurements were performed in triplicate and data are means with standard deviation < 12 %. As a positive control daunorubicin was used and an IC_{50} value of 12.55 ± 0.07 μM was obtained.

4.7. Molecular modeling

Protein preparation

Protein structures for the PI3K-alpha mutant and the human ATR-ATRIP complex were retrieved from the Protein Databank (PDB) and prepared using the Protein Preparation Wizard tool in Schrödinger software, version 2021-4 (Schrödinger, LLC, New York, NY, USA) [36]. The human ATR-ATRIP complex (PDB-ID: 5YZ0) represents the apo-form, while the PI3K-alpha mutant (PDB-ID: 5UL1) is complexed with a 2-aminopyrazine inhibitor [23]. In both structures only chain A was retained during preparation. Water molecules were removed, and the structures were prepared by adding missing hydrogen atoms and side chains. The hydrogen-bonding network was optimized using PROPKA (Schrödinger, LLC, New York, NY, USA) at pH 7.0 [37]. Finally, restrained minimization was performed employing the OPLS4 force-field and RMSD cutoff of 0.3 Å for heavy atoms [38].

4.7.2. Ligand preparation

All ligand structures were prepared using the LigPrep panel and the OPLS4 force-field available in Schrödinger software, version 2021-4. At pH 7.0 ± 1.0, different ionization states were produced applying Epik in Schrödinger software [37]. Subsequently, the ConfGen tool in Schrödinger software was implemented to generate and minimize a maximum of 64 ligand conformations per compound [39].

4.7.3. Homology model generation

A homology model of the catalytic domain of ATR was generated with the MODELLER program, using the crystal structure of PI3K-alpha mutant in complex with a 2-aminopyrazine inhibitor (PDB-ID: 5UL1) [40]. The ATP-binding site of both proteins shows 61.3 % sequence similarity and 43.5 % identity.

The amino acid sequence of the catalytic domain of ATR was retrieved from Uniprot (amino acid from 2290 to 2644). Sequence and structural alignment was performed in MOE (Molecular Operating Environment 2022.02, Chemical Computing Group ULC, 1010 Sherbooke St. West, Suite #910, Montreal, QC, Canada) on prepared protein structure of PI3K-alpha mutant (PDB-ID: 5UL1) and the catalytic domain of ATR (PDB-ID: 5YZ0). Subsequently, the obtained alignment was used to generate the homology model. The Leu766 and Leu279 residue area was chosen for model creation. Flexible loops that pose challenges in the creation of the homology model were manually removed. Finally, 20 models were generated and the best one was determined by using the DOPE energy and GA341 score [41]. The best scored model was prepared with the Protein Preparation Wizard after adding the cocrystallized ligand.

4.7.4. Molecular docking

The cocrystallized ligand in the protein structures 5UL1 and the ATR model was used as the centre of the receptor grid box constructed with the size of 10 x 10 × 10 Å using the Receptor Grid Generation tool. For

molecular docking, Glide (Schrödinger, LLC, New York, NY, USA) with Standard Precision mode was utilized [42]. Validation of the developed homology model of ATR and the employed methods was performed by redocking the cocrystallized ligand into both protein structures. Glide was able to correctly replicate the binding mode of the ligand in the structures, with RMSD values of 1.5 Å. A limit of 100 poses per ligand was chosen for post-docking minimization. The obtained poses were ranked using the docking score. Then, the top-scored docking poses were visually inspected, focusing mainly on the interaction between the ligand and the kinase hinge region. Obtained docking scores of studied inhibitors are shown in Tables S2 and S2 in the Supplement.

Funding

This work was funded by the Deutsche Forschungsgemeinschaft (DFG) project number 468534282 (FOR 5433 to W.S.), 528202295 and 495271833 (to W.S and O.H.K, 427404172, 445785155, 469954457, 496927074, 502534123, 528202295, 393547839 (SFB 1361). 318346496 (SFB1292) (to O.H.K). Further support is acknowledged from DAAD Egypt/Germany, the Brigitte und Dr. Konstanze Wegener-Stiftung (project 65/110) and the Walter Schulz-Stiftung (O.H.K).

CRediT authorship contribution statement

Abdallah M. Alfayomy: Investigation, Methodology, Writing – original draft. **Ramy Ashry:** Formal analysis, Investigation, Methodology, Writing – original draft. **Anita G. Kansy:** Formal analysis, Investigation, Methodology. **Anne-Christin Sarnow:** Formal analysis, Investigation, Methodology. **Frank Erdmann:** Formal analysis, Investigation, Methodology. **Matthias Schmidt:** Formal analysis, Investigation, Methodology, Validation. **Oliver H. Krämer:** Conceptualization, Data curation, Funding acquisition, Project administration, Supervision, Writing – review & editing. **Wolfgang Sippl:** Conceptualization, Data curation, Funding acquisition, Resources, Supervision, Writing – review & editing.

Declaration of competing interest

The authors declare that they have no known competing financial interests or personal relationships that could have appeared to influence the work reported in this paper.

Data availability

Data will be made available on request.

Appendix A. Supplementary data

Supplementary data to this article can be found online at https://doi.org/10.1016/j.ejmech.2024.116167.

References

[1] T. Nikolova, N. Kiweler, O.H. Krämer, Interstrand crosslink repair as a target for HDAC inhibition, Trends Pharmacol. Sci. 38 (2017) 822–836.
[2] N.Y. Ngoi, M.M. Pham, D.S. Tan, T.A. Yap, Targeting the replication stress response through synthetic lethal strategies in cancer medicine, Trends Cancer 7 (2021) 930–957.
[3] O.L. Kantidze, A.K. Velichko, A.V. Luzhin, N.V. Petrova, S.V. Razin, Synthetically lethal interactions of ATM, ATR, and DNA-PKcs, Trends Cancer 4 (2018) 755–768.
[4] J.S. Baxter, D. Zatreanu, S.J. Pettitt, C.J. Lord, Resistance to DNA repair inhibitors in cancer, Mol. Oncol. 16 (2022) 3811–3827.
[5] A.A.B. da Costa, D. Chowdhury, G.I. Shapiro, A.D. D'Andrea, P. A. Konstantinopoulos, Targeting replication stress in cancer therapy, Nat. Rev. Drug Discov. 22 (2023) 38–58.
[6] E. Lecona, O. Fernandez-Capetillo, Targeting ATR in cancer, Nat. Rev. Cancer 18 (2018) 586–595.
[7] P.M. Reaper, M.R. Griffiths, J.M. Long, J.-D. Charrier, S. MacCormick, P. A. Charlton, J.M. Golec, J.R. Pollard, Selective killing of ATM-or p53-deficient cancer cells through inhibition of ATR, Nat. Chem. Biol. 7 (2011) 428–430.
[8] J.-D. Charrier, S.J. Durrant, J.M.C. Golec, D.P. Kay, R.M.A. Knegtel, S. MacCormick, M. Mortimore, M.E. O'Donnell, J.L. Pinder, P.M. Reaper, A. P. Rutherford, P.S.H. Wang, S.C. Young, J.R. Pollard, Discovery of potent and selective inhibitors of ataxia telangiectasia mutated and Rad3 related (ATR) protein kinase as potential Anticancer agents, J. Med. Chem. 54 (2011) 2320–2330.
[9] R. Prevo, E. Fokas, P.M. Reaper, P.A. Charlton, J.R. Pollard, W.G. McKenna, R. J. Muschel, T.B. Brunner, The novel ATR inhibitor VE-821 increases sensitivity of pancreatic cancer cells to radiation and chemotherapy, Cancer Biol. Ther. 13 (2012) 1072–1081.
[10] R. Jossé, S.E. Martin, R. Guha, P. Ormanoglu, T.D. Pfister, P.M. Reaper, C.S. Barnes, J. Jones, P. Charlton, J.R. Pollard, J. Morris, J.H. Doroshow, Y. Pommier, ATR inhibitors VE-821 and VX-970 sensitize cancer cells to topoisomerase I inhibitors by Disabling DNA replication initiation and fork elongation responses, Cancer Res. 74 (2014) 6968–6979.
[11] C.J. Huntoon, K.S. Flatten, A.E. Wahner Hendrickson, A.M. Huehls, S.L. Sutor, S. H. Kaufmann, L.M. Karnitz, ATR inhibition broadly sensitizes ovarian cancer cells to chemotherapy independent of BRCA status, Cancer Res. 73 (2013) 3683–3691.
[12] R. Knegtel, J.-D. Charrier, S. Durrant, C. Davis, M. O'Donnell, P. Storck, S. MacCormick, D. Kay, J. Pinder, A. Virani, Rational design of 5-(4-(Isopropylsulfonyl) phenyl)-3-(3-(4-((methylamino) methyl) phenyl) isoxazol-5-yl) pyrazin-2-amine (VX-970, M6620): optimization of intra-and intermolecular polar interactions of a new ataxia telangiectasia mutated and Rad3-related (ATR) kinase inhibitor, J. Med. Chem. 62 (2019) 5547–5561.
[13] A. Thomas, C.E. Redon, L. Sciuto, E. Padiernos, J. Ji, M.-J. Lee, A. Yuno, S. Lee, Y. Zhang, L. Tran, Phase I study of ATR inhibitor M6620 in combination with topotecan in patients with advanced solid tumors, J. Clin. Oncol. 36 (2018) 1594.
[14] L. Gorecki, M. Andrs, M. Rezacova, J. Korabecny, Discovery of ATR kinase inhibitor berzosertib (VX-970, M6620): clinical candidate for cancer therapy, Pharmacol. Ther. 210 (2020) 107518.
[15] A. Hanzl, G.E. Winter, Targeted protein degradation: current and future challenges, Curr. Opin. Chem. Biol. 56 (2020) 35–41.
[16] Y.-W. Wang, L. Lan, M. Wang, J.-Y. Zhang, Y.-H. Gao, L. Shi, L.-P. Sun, PROTACS: a technology with a gold rush-like atmosphere, Eur. J. Med. Chem. 247 (2023) 115037.
[17] A.-H.M. Mustafa, O.H. Krämer, Pharmacological modulation of the crosstalk between aberrant janus kinase signaling and epigenetic modifiers of the histone deacetylase family to treat cancer, Pharmacol. Rev. 75 (2023) 35–61.
[18] B. Sun, W. Fiskus, Y. Qian, K. Rajapakshe, K. Raina, K. Coleman, A. Crew, A. Shen, D. Saenz, C. Mill, BET protein proteolysis targeting chimera (PROTAC) exerts potent lethal activity against mantle cell lymphoma cells, Leukemia 32 (2018) 343–352.
[19] G.M. Burslem, B.E. Smith, A.C. Lai, S. Jaime-Figueroa, D.C. McQuaid, D. P. Bondeson, M. Toure, H. Dong, Y. Qian, J. Wang, The advantages of targeted protein degradation over inhibition: an RTK case study, Cell Chem. Biol. 25 (2018) 67–77.
[20] M. He, C. Cao, Z. Ni, Y. Liu, P. Song, S. Hao, Y. He, X. Sun, Y. Rao, PROTACs: great opportunities for academia and industry (an update from 2020 to 2021), Signal Transduct. Target Ther. 7 (2022) 181.
[21] D. Chirnomas, K.R. Hornberger, C.M. Crews, Protein degraders enter the clinic—a new approach to cancer therapy, Nature Rev. Clin. Oncol. 20 (2023) 265–278.
[22] D. Menolfi, S. Zha, ATM, ATR and DNA-PKcs kinases—the lessons from the mouse models: inhibition≠ deletion, Cell Biosci. 10 (2020) 1–15.
[23] Y. Lu, M. Knapp, K. Crawford, R. Warne, R. Elling, K. Yan, M. Doyle, G. Pardee, L. Zhang, S. Ma, M. Mamo, E. Ornelas, Y. Pan, D. Bussiere, J. Jansen, I. Zaror, A. Lai, P. Barsanti, J. Sim, Rationally designed PI3Kα mutants to mimic ATR and their use to understand binding specificity of ATR inhibitors, J. Mol. Biol. 429 (2017) 1684–1704.
[24] Q. Rao, M. Liu, Y. Tian, Z. Wu, Y. Hao, L. Song, Z. Qin, C. Ding, H.-W. Wang, J. Wang, Y. Xu, Cryo-EM structure of human ATR-ATRIP complex, Cell Res. 28 (2018) 143–156.
[25] T. Ishiyama, M. Murata, N. Miyaura, Palladium (0)-catalyzed cross-coupling reaction of alkoxydiboron with haloarenes: a direct procedure for arylboronic esters, J. Org. Chem. 60 (1995) 7508–7510.
[26] C.M. Camacho, M.G. Pizzio, D.L. Roces, D.B. Boggián, E.G. Mata, Y. Bellizzi, E. Barrionuevo, V.C. Blank, L.P. Roguin, Design, synthesis and cytotoxic evaluation of a library of oxadiazole-containing hybrids, RSC Adv. 11 (2021) 29741–29751.
[27] D.S. Mortensen, S.M. Perrin-Ninkovic, R. Harris, B.G.S. Lee, G. Shevlin, M. Hickman, G. Khambatta, R.R. Bisonette, K.E. Fultz, S. Sankar, Discovery and SAR exploration of a novel series of imidazo[4,5-b]pyrazin-2-ones as potent and selective mTOR kinase inhibitors, Bioorg. Med. Chem. Lett. 21 (2011) 6793–6799.
[28] X. Jiang, J. Zhou, Y. Wang, X. Liu, K. Xu, J. Xu, F. Feng, H. Sun, PROTACs suppression of GSK-3β, a crucial kinase in neurodegenerative diseases, Eur. J. Med. Chem. 210 (2021) 112949.
[29] B. Zhou, J. Hu, F. Xu, Z. Chen, L. Bai, E. Fernandez-Salas, M. Lin, L. Liu, C.-Y. Yang, Y. Zhao, Discovery of a small-molecule degrader of bromodomain and extra-terminal (BET) proteins with picomolar cellular potencies and capable of achieving tumor regression, J. Med. Chem. 61 (2018) 462–481.
[30] Y. Li, J. Yang, A. Aguilar, D. McEachern, S. Przybranowski, L. Liu, C.-Y. Yang, M. Wang, X. Han, S. Wang, Discovery of MD-224 as a first-in-class, highly potent, and efficacious proteolysis targeting chimera murine double minute 2 degrader capable of achieving complete and durable tumor regression, J. Med. Chem. 62 (2019) 448–466.
[31] J. Zhang, J. Che, X. Luo, M. Wu, W. Kan, Y. Jin, H. Wang, A. Pang, C. Li, W. Huang, Structural feature analyzation strategies toward discovery of orally bioavailable

PROTACs of Bruton's tyrosine kinase for the treatment of lymphoma, J. Med. Chem. 65 (2022) 9096–9125.
[32] J. Min, A. Mayasundari, F. Keramatnia, B. Jonchere, S.W. Yang, J. Jarusiewicz, M. Actis, S. Das, B. Young, J. Slavish, Phenyl-glutarimides: alternative cereblon binders for the design of PROTACs, Angew. Chem. Int. Ed. 60 (2021) 26663–26670.
[33] X. Han, C. Wang, C. Qin, W. Xiang, E. Fernandez-Salas, C.-Y. Yang, M. Wang, L. Zhao, T. Xu, K. Chinnaswamy, Discovery of ARD-69 as a highly potent proteolysis targeting chimera (PROTAC) degrader of androgen receptor (AR) for the treatment of prostate cancer, J. Med. Chem. 62 (2019) 941–964.
[34] H. Schumacher, R. Smith, R. Williams, The metabolism of thalidomide: the fate of thalidomide and some of its hydrolysis products in various species, Br. J. Pharmacol. Chemother. 25 (1965) 338.
[35] R. Ashry, A.-H.M. Mustafa, K. Hausmann, M. Linnebacher, S. Strand, W. Sippl, M. Wirth, O.H. Krämer, NOXA accentuates apoptosis induction by a novel histone deacetylase inhibitor, Cancers 15 (2023) 3650.
[36] G. Madhavi Sastry, M. Adzhigirey, T. Day, R. Annabhimoju, W. Sherman, Protein and ligand preparation: parameters, protocols, and influence on virtual screening enrichments, J. Comput. Aided Mol. Des. 27 (2013) 221–234.
[37] J.C. Shelley, A. Cholleti, L.L. Frye, J.R. Greenwood, M.R. Timlin, M. Uchimaya, Epik: a software program for pKaprediction and protonation state generation for drug-like molecules, J. Comput. Aided Mol. Des. 21 (2007) 681–691.
[38] C. Lu, C. Wu, D. Ghoreishi, W. Chen, L. Wang, W. Damm, G.A. Ross, M.K. Dahlgren, E. Russell, C.D. Von Bargen, R. Abel, R.A. Friesner, E.D. Harder, OPLS4: improving force field accuracy on challenging regimes of chemical space, J. Chem. Theor. Comput. 17 (2021) 4291–4300.
[39] K.S. Watts, P. Dalal, R.B. Murphy, W. Sherman, R.A. Friesner, J.C. Shelley, ConfGen: a conformational search method for efficient generation of bioactive conformers, J. Chem. Inf. Model. 50 (2010) 534–546.
[40] M.-y.S. Eramian, U. Pieper, A. Sali, Comparative protein structure modeling using modeller, Current Protocols in Bioinformatics 5 (2006) 1–5, 6.
[41] D. Eramian, N. Eswar, M.-Y. Shen, A. Sali, How well can the accuracy of comparative protein structure models be predicted? Protein Sci. 17 (2008) 1881–1893.
[42] R.A. Friesner, R.B. Murphy, M.P. Repasky, L.L. Frye, J.R. Greenwood, T.A. Halgren, P.C. Sanschagrin, D.T. Mainz, Extra precision Glide: docking and scoring incorporating a model of hydrophobic enclosure for Protein−Ligand complexes, J. Med. Chem. 49 (2006) 6177–6196.